Ames File

NASA TECHNICAL MEMORANDUM

NASA TM X-62,459

NASA TM X-62,459

FLOW VISUALIZATION OF VORTEX INTERACTIONS IN MULTIPLE VORTEX WAKES BEHIND AIRCRAFT

D. L. Ciffone and C. Lonzo, Jr.

Ames Research Center
Moffett Field, Calif. 94035

June 1975

1. Report No.	2. Government Accession No.	3. Recipient's Catalog No.
TM X-62,459		

4. Title and Subtitle	5. Report Date
FLOW VISUALIZATION OF VORTEX INTERACTIONS IN MULTIPLE VORTEX WAKES BEHIND AIRCRAFT	6. Performing Organization Code
7. Author(s) D. L. Ciffone and C. Lonzo, Jr.	8. Performing Organization Report No. A-6193
9. Performing Organization Name and Address Ames Research Center Moffett Field, California 94035	10. Work Unit No.
	11. Contract or Grant No.
12. Sponsoring Agency Name and Address National Aeronautics and Space Administration Washington, D. C. 20546	13. Type of Report and Period Covered Technical Memorandum
	14. Sponsoring Agency Code

15. Supplementary Notes

16. Abstract

A flow visualization technique has been developed which allows the nature of lift-generated wakes behind aircraft models to be investigated. The technique has been applied to models being towed underwater in a ship model basin. Seven different configurations of a small-scale model of a 747 transport aircraft were used to allow observation of typical vortex interactions and merging in multiple vortex wakes. It was established that the motion of the wake vortices is often sensitive to small changes in either wing span loading or model attitude. Landing gear deployement was found to cause a far-field reformation of vorticity behind a model configuration which dissipated concentrated vorticity in the near-field wake. Alleviation of wake vorticity is achievable by configuring the wing span loading to cause the wake vortices to move in paths that result in their interactions and merging. The vortices shed from the horizontal stabilizer always moved down rapidly into the wake and merged with the other vortices, primarily the inboard flap vortices.

17. Key Words (Suggested by Author(s))	18. Distribution Statement
Vortex interactions Merging Multiple vortex valves	Unclassified - Unlimited STAR Category ~~48,99~~ 02,34

19. Security Classif. (of this report)	20. Security Classif. (of this page)	21. No. of Pages	22. Price*
Unclassified	Unclassified	59	$4.25

*For sale by the National Technical Information Service, Springfield, Virginia 22151

TABLE OF CONTENTS

SYMBOLS

$\bar{c}$	mean aerodynamic chord
C_{D_i}	theoretically estimated induced drag coefficient
C_{L_E}	measured lift coefficient
Clean	cruise configuration, no surfaces deflected
C_{L_T}	theoretically estimated lift coefficient
D_F	measured distance between vortices from the outboard edge of the inboard flaps
D_{F_O}	initial measurement of distance between inboard flap outer edge vortices
D_V	measured vertical distance between highest position of wing tip vortex above wing and subsequent positions
D_W	measured distance between wing tip vortices
D_{W_O}	initial measurement of distance between wing tip vortices
GD	gear down
GU	gear up
i_t	tail incidence, deg
i_w	wing incidence, deg
LDG	landing configuration, inboard and outboard flaps deflected 46 deg, leading edge flaps deployed
LDG/O	same as LDG but with outboard flaps retracted
MOD LDG	same as *LDG* but with 30 percent of inboard span of inboard flap removed
MOD LDG/O	same as *LDG/O* but with 30 percent of inboard span of inboard flap removed
MOD LDG/T.O.	same as *MOD LDG/O* but with outboard flaps deflected 7 deg
T.O.	take off configuration, inboard and outboard flaps deflected 7 deg, leading edge flaps deployed
U_∞	towing speed, m/sec

X/b	downstream distance in span lengths
α	model angle of attack, deg
α_t	tail angle of attack, deg
α_w	wing angle of attack, deg
Δ	measured distance between vortices from the wing tip and outer edge of inboard flap
ϵ	downwash angle, deg
ϕ	angle of rotation of wing tip vortex about flap vortex, deg
ψ	angle of yaw, deg

FLOW VISUALIZATION OF VORTEX INTERACTIONS IN MULTIPLE VORTEX WAKES BEHIND AIRCRAFT

D.L. Ciffone and C. Lonzo, Jr.

Ames Research Center

INTRODUCTION

Theoretical studies (refs. 1-2) have indicated that by modifying the wing span loading of an aircraft, a significant reduction in the rotational velocities within its wake are achievable. The studies were verified in ground-based experiments both on the conceptual level (ref. 3) and in application to a 747-type transport model (ref. 4). However, recent flight tests (ref. 5) have indicated that, although the span loading can be modified to substantially reduce wake rotational velocities, the deployment of landing gear and/or yawing motions of the aircraft can substantially reduce the benefits of span load alterations. Subsequent wind-tunnel tests did not identify visual differences, or could velocity or induced rolling moment differences, on a following model due to deployment of landing gear of the wake generating model. Consequently, it was decided to develop a flow visualization technique to be used in a water tow-tank (ship model basin) to allow better understanding of the vortex interactions and merging characteristics in multiple vortex wakes. In particular, the tow-tank was selected to allow the far field wake to be examined for differences in wake vorticity as a result of landing gear deployment.

The tests were performed in the University of California's water tow-tank facility at Richmond, California. In this method of testing, the model is towed underwater, generating a continuous wake which decays with time at each longitudinal point of the test gallery. The only restriction to test time comes from either the ultimate interference from walls or floor, or the passage through the test section of internal vortex waves, which arise from starting or stopping of the model at the beginning and end of the towing range. Previous tests in this facility allowed measurements of wake velocities to 200-span lengths behind the model (refs. 3 and 6).

Comprehensive photographic results were obtained of the wake of a 0.01 scale model of a 747 transport with various wing span loadings in both the landing gear up and down configurations. The model was internally equipped with a dye-ejection system which marked the multiple vortices in its wake. Different configurations were tested; angle of attack, tail incidence, yaw and towing speed were varied. Reynolds number based on model span, at a towing speed of 2 m/sec, was 1.2 million. The results cover a large portion of the time history of vortex interactions typical of multiple vortex wakes shed by transport type aircraft. They will be used to update existing wake vortex models and guide the development of future theoretical models. All of the film has been cataloged for future viewing. Some of the footage of greatest interest has been edited and prints made for presentation purposes.

MODEL AND APPARATUS

Facility Description

The test facility was the University of California's water tow-tank located in Richmond, California. The tank is 61 m long, 2.44 m wide, and 1.7 m deep. However, only a 35-m length was utilized. A carriage operator rode an electrically-driven carriage, from which the model and connecting strut were suspended. The model was towed through the tank at speeds up to 2 m/sec. A photosensitive timing system mounted on the carriage structure provided an accurate selection and speed readout. The model was towed past a viewing station located approximately 14 m from the starting point of the carriage and 21 m from the stopping location. Four 1-m-wide glass windows at this station extend from a point approximately 0.6 m above the bottom of the tank to well above the free surface. Figure 1 shows the model passing three of the test station windows during a test run.

Model Description

The flow studies were conducted with a 0.01 scale model of a Boeing 747 transport aircraft. Principal geometric characteristics of the model are presented in table 1.

The model is made of aluminum with an external surface an anodized gold color. The model was constructed from drawings and templates of an existing 0.03 scale wind tunnel model. Installed internally are a mounting bracket and stainless steel and plastic dye tubes which were constructed to be compatible with the model strut and flow visualization systems. The dye tube orifices were located at the wing tips, the outboard and inboard edges of the inboard flaps and at the tips of the horizontal stabilizer. The incidence angle of the horizontal stabilizer could be varied from $+4^\circ$ to -4°. The model was equipped with leading edge flaps and triple-slotted trailing edge flaps. Nose, fuselage and wing landing gear (constructed of stainless steel, brass and rubber) were used to investigate the effects of the landing gear.

Figure 2 shows the trailing edge flap geometry. Figures 3 and 4 show the landing configuration model with the flaps and landing gear details.

FLOW VISUALIZATION

To obtain an adequate means of observing the vortices in the model's trailing wake, the model was equipped with a sophisticated dye-ejection system. Eight dye-ejection orifices were positioned on the model at the following locations: each wing tip, the inboard and outboard edges of the inboard flaps, and the tips of the horizontal stabilizer. The dye orifices were connected via internal tubes through the model and model strut to a pressurized reservoir. Manifolds and solenoid activated valves were used to release various combinations of dye traces from the model. The reservoir (fig. 5) was mounted on the overhead carriage, and the solenoid valves were activated by the carriage operator.

A viewing station, which consists of four large glass windows, was used as the primary means for obtaining photographic coverage of the flow phenomena. This area of the water tank was equipped with a background grid on the floor and wall opposite the windows, and twelve 500-watt underwater flood lights (fig. 6). The background was black with white grid lines forming 61-cm squares. The dye-marked vortices were photographed in three separate ways: by a 16-mm DBM camera with a 10-mm lens mounted below the free surface looking downstream and downward into the viewing station (first viewing the streaming vortices and later viewing a cross section through the wake); and by two 16-mm DBM cameras, one with a 10-mm lens and the other with a 25-mm lens, both mounted outside the tank photographing the streaming vortices from the side. The side camera with the 25-mm lens was positioned close to one test station window and filmed local wake detail; the second camera with the 10-mm lens was positioned far enough from the test station windows to obtain a panoramic view of the wake across three of the windows.

It was initially planned to have the underwater camera and side cameras time-synchronized. However, the placement of the underwater lights for optimal illumination of the wake was radically different for underwater and side viewing; consequently the wake was filmed in two steps. First, all of the underwater tests were filmed and then, the lights were repositioned and the tests were repeated and filmed from the side.

In addition to the 16-mm motion films, key portions of the test were photographed using a hand-held 35-mm single-lens reflex (SLR) camera viewing the wake detail from the side through the windows and from above through the free surface.

A cross-section through the wake (a Trefftz Plane view) was also filmed by the underwater 16-mm camera and the hand-held SLR. An 800-watt xenon arc lamp was used with a specially-designed lens and light slit system to shine a high-intensity, thin light sheet across the towing tank. All other lights at the facility were turned off, and the illuminated slice through the wake was photographed.

Table 2 lists the model configurations tested and the film coverage by run number. Table 3 summarizes the pertinent camera data and types of film used.

PROCEDURE AND DATA ACQUISITION

Experimental Procedure

The Reynolds number was 1.2 million based on wing span and a towing speed of 2 m/sec. The model centerline was located approximately five chord lengths (0.75 of a span) below the free surface. It has been concluded that the scaling laws for modeling fluid phenomena, pertinent to the study of wake vortices, are essentially the same for tests in water as in air (ref. 7). Air compressibility effects on vortex behavior are negligible as long as the full scale aircraft mach numbers are typical of holding or landing flight speeds. No visible cavitation was observed during the tests. Froude number, the ratio of inertial to gravitational forces, is used as the basis for scaling in hydrodynamic model tests where free-surface effects are of interest. However, it has been shown (ref. 8) that the forces acting on hydrofoils operated at depths greater than two chord lengths are essentially unaffected by the free surface and are equal to those obtained on a wing operating in an

infinite medium. The free surface does, however, act as a reflection plane and corrections to vortex trajectories may be necessary.

The main purpose of this test was to develop and use flow visualization as a tool to investigate vortex interactions in multiple vortex wakes. Different wake characteristics were generated by changing both the attitude and flap geometry of a 0.01 scale model of a 747 transport. Both 16-mm and 35-mm cameras were used to document the vortex interaction as the wake aged.

Prior to each test run, the model geometry and attitude was selected, the dye-ejection system was loaded with water and yellow and pink fluorescent dyes (which appear as green and orange during the test), and the manifold valves were preset to eject dye for selected ports. The desired lighting was set, the towing carriage was started and brought up to a selected speed, and dye ejection was begun by electrically operated solenoid valves. As the model approached the viewing section of the tank, the cameras were simultaneously activated by a single manual switch. A clock, viewed by one of the cameras, was used for determining vortex age. The 35-mm hand-held camera was operated at a constant frame speed; vortex age was then determined from the photographs through knowledge of the towing speed. The carriage then continued at constant speed to its stopping position 35 wing spans beyond the viewing station. At this distance, disturbances due to motion waves did not propagate back to the test area during the data gathering interval (ref. 3). Immediately after obtaining all photographic data, the underwater flood lights were extinguished to minimize the formation of thermally-induced convective currents in the tank, and the carriage was returned to the starting end of the tank for a 15-30-minute wait for water motion to settle out prior to the next run.

The tank was chlorinated prior to and during the tests to keep the water clear and free from dye accumulation. In addition, the water was continuously cycled and filtered.

Data Acquisition and Presentation

Typical flow visualization data obtained during this test are shown in figures 7 through 12. Results from the underwater camera viewing the streaming vortices are presented in figure 7. A side view of the streaming vortices and of a cross section of the wake in the light sheet are shown in 35-mm photos (figs. 8-12). This type of photographic information provides a qualitative understanding of the interactions of vortices in multiple vortex wakes. In addition, changes in vortex positions as the wake aged were obtained from the photographs by correcting both camera viewing and cone angles. Examples of vortex trajectories and trajectory parameters thus obtained are presented in figures 15 through 34.

RESULTS AND DISCUSSION

Seven different configurations of the 747 model were tested. Table 4 summarizes the configurations and angles of attack that were investigated. Also listed in the table are the test lift coefficients as predicted by vortex lattice theory (ref. 9) C_{L_T}, and as measured in a wind tunnel (ref. 4) C_{L_E}. The effect of model yaw and tail incidence on wake characteristics were also explored as indicated in the table. As an aid to the discussion that follows, the spanwise lift

distributions for the configurations of table 4 are presented as each configuration is discussed. These span loadings were calculated from vortex lattice theory (ref. 9). In this section of the report, the nature of the wake that was observed behind each of the configurations will be discussed separately.

Clean Configuration

The clean configuration consisted of all flaps at zero deflection, landing gear retracted, and leading edge slats on. This configuration represents aircraft cruise. Vortices are shed from the wing tips. At the 5.8° angle of attack, these tip vortices had tight cores and were quite straight. At both the 2.9° and 10° angles of attack, they were more diffuse and assumed a sinusoidal shape in the longitudinal direction. The reason for this at the lower angle of attack is the reduced lift; at the higher angle, the swept wing was probably experiencing some tip stall. The vortices of this configuration were quite persistent. The dye from the horizontal stabilizer tip vortices was seen to descend, swing out and wrap around the wing tip vortices. If motions in the tank were not allowed to settle out prior to each test run, Crow instabilities (ref. 10) could be excited in the wake.

The wing span load distribution determines the number, strength, and location of vortices in the wake of the wing. The elliptic span loading of the swept wing is shown in figure 13. The isolated vortex shed from each side of the wing is a result of the load gradient at the wing tips. The loadings of this figure can be used for comparison purposes with the other test configurations of the model.

Take-off Configuration

The take-off configuration consisted of all flaps, trailing edges deflected down 7° (fig. 2), landing gear deployed and leading edge slats on. Five vortices are shed from each side of the wing; four from the flap edges, and one vortex from the wing tip. This vortex grouping might appear obvious from the wing span loading shown in figure 14. The vortex interactions were found to be basically the same for both investigated angles of attack (5.8° and 8°). The wing tip vortices moved upward and inboard. At 11 spans their initial separation distance was reduced by about 40 percent, and remained constant to about 28 spans, where tank bottom effects then caused them to start separating again (figs. 9 and 15). The photographs indicated that the fluctuation in separation distance at $2.5 \leq X/b \leq 4$ is due to the merging of the outboard flap outer edge vortex with the wing tip vortex. At approximately six to eight spans the upward movement of the tip vortices was replaced with a constant sink rate of 6.4 cm/sec for the model at an 8° angle of attack, and 4.0 cm/sec for the 5.8° angle of attack (fig. 16). These sink rates remained constant until the vortices were influenced by the bottom of the tank, where the rate of sink began to be arrested.

The dye marking of the vortices at the edges of the inboard flap indicated that the flap vortex system moves downward immediately after formation. The outer edge vortex appears to rotate up over the inner edge vortex and the pair merges with the inner flap pair from the other side of the model (fig. 9). Prior to this merging, the tip vortex from the horizontal stabilizer sinks rapidly downward and violently interacts with the outer edge flap vortex, causing an elongation of the dye pattern marking this flap vortex. This interaction occurs at 2.5 spans. Complete merging of the flap vortices is achieved by 4.5 spans.

The wing tip vortices of this configuration remain apart from the flap and horizontal vortex merging below the model centerline (fig. 9). They were quite persistent and remained evident in the tank well after the 40 spans that were visible in the light sheet.

Landing Configuration

The landing configuration consisted of all flaps, trailing edges deflected down 46° (fig. 2), landing gear deployed and leading edge slats on. Five vortices were shed from each side of the wing; four from the flap edges, and one from the wing tip. The predicted wing span loading for this configuration is presented in figure 17. The model was tested at an angle of attack of 2.9° simulating a landing lift coefficient of 1.2. The wing tip vortices moved upward and inboard, and at two spans begin to merge with the vortex from the outboard edge of the outboard flap. The tip vortex rapidly orbits from above and inboard of the flap vortex and completely merges with it by 3.5 spans. The result is a persistent single vortex (fig. 10). Upon examination of the span load distribution (fig. 17), this result is not surprising; the steep load gradient associated with the outer edge of the outboard flap might be expected to dominate the tip vortex of like sign. Once these merged vortices form on each side of the wing, the distance which separates them gradually increases and their sink rate remains constant, until they approach the bottom of the tank (fig. 18).

Both the resulting vortex from between the flaps and the inner flap inboard edge vortex appeared to be quite diffuse (fig. 10). At a little over one span behind the model, the vortices shed from the horizontal stabilizer passed through this vortex doublet. By 2.5 spans there was complete merging of the flap and tail vortices. The result was a diffuse cloud of dye near the centerline of the model wake. The merged outer edge flap vortices of the outboard flaps remained apart from the inboard flap and horizontal tail vortex merging, and persisted in the tank well after the 40 spans that they were visible in the light sheet. No noticeable difference in the wake characteristics was observed when the landing gear were retracted.

LDG/O Configuration

The *LDG/O* configuration consisted of the inboard flaps, trailing edges deflected down 46° and the outboard flaps set at zero deflection. The leading edge slats were on and the model wake was viewed both with landing gear deployed and retracted. Wakes were generated with the model at 2.9°, 5.8° and 8° angles of attack. This configuration was tested because theoretically (refs. 1 and 2) and experimentally (refs. 4 and 5), it was found to result in an alleviation of the persistent wake associated with the landing configuration. The span loading predicted from vortex lattice theory is presented in figure 19. At angles of attack of 5.8° and 8°, the vortex associated with the steep gradient in span loading at the outboard edge of the flap was the dominant vortex of the three vortices shed from each side of the wing. Under its influence the vortex from the inboard side of the flap was rotated to a position directly below it, and the wing tip vortex moved up, inboard, and then down to orbit about and merge with this outboard edge flap vortex (fig. 11).

The effect of landing gear on wake characteristics was investigated at 5.8° angle of attack. With the gear retracted, the following sequence of events occurred in the wake: (1) at one span downstream, the vortex from the tip of the horizontal tail descended between the vortex pair from the flap, (2) by three spans the tail vortex had merged with the flap vortices, merging primarily

consisting of the tail vortex wrapping up around the outboard side of the flap outer edge vortex, (3) in six spans the flap inboard edge vortex had rotated downward and outboard to a position directly below the outer edge flap vortex, (4) the wing tip vortices had moved up and inboard and then moved down between the two outer edge flap vortices and began to orbit around them, (5) at 13 spans the wing and flap vortices merged, and (6) by 20 span lengths there was no distinguishable vortices in the wake; only two diffuse clouds of dye remained.

With the landing gear deployed (fig. 11), the following changes in the wake were noted: (1) the flap vortices initially appeared to be more diffuse, (2) the horizontal tail and flap merging was almost entirely between the tail vortex and the outer edge flap vortex, (3) the wing tip vortex merged with the outer edge flap vortex sooner (at 11 spans), (4) by 20 spans the wake consisted of two diffuse clouds which were not as elongated or diffuse as the retracted gear situation and (5) by 40 spans the diffuse clouds began to collapse into small areas again and seemed to reform into vortices.

A comparison of wing tip trajectories in the near field for the *LDG/O* configuration with gear up and down at an angle of attack of 5.8°, is presented in figures 20 through 23. The relative angular position of the right wing tip vortex about the right flap outer edge vortex as a function of downstream distance is shown in figure 20. The zero reference is a line passing through both outer edge flap vortices. The wing tip vortex moves up and inboard about the flap vortex at an angular rate of 23 deg/sec to an angular position of about 100° as it begins to swing down between the two outboard flap vortices and sees the wing tip vortex from the opposite side, it accelerates to 53 deg/sec. It maintains this rate to about 225° (8.5 spans) where it decelerates to its original rate of 23 deg/sec. With the gear down, the tip vortex orbits about the flap vortex at a slightly higher rate and merges sooner (11 spans as compared to 13).

The relative separation distance of the right side wing tip vortex from the flap vortex as a function of downstream distance is presented in figure 21. As the tip vortex moves up and inboard, it approaches closer to the flap vortex until it reaches the 180° position (7 spans downstream). At this position both tip vortices lie between the flap vortices on a straight line adjoining the flap vortices. The distance then begins to increase until the tip and flap vortices merge at about 11 to 13 spans downstream. Until an angular position of 210° is achieved ($\sim$ 8 spans), there is little if any difference in separation distance attributable to landing gear. Beyond 210°, the separation distance is less for the gear-down configuration. The distance between wing tip vortices as a function of downstream distance for the same configurations is presented in figure 22. The distance decreases as the tip vortices move inboard, and reaches a minimum after rotation through an angle of 180° about the flap vortices (7 spans downstream). Up to that time there is no discernible gear effects; however, as the merging process continues, the distance between tip vortices begins to increase, with a rate twice as great for the gear-down configuration.

Figure 23 shows the spiral trajectory of the right wing tip vortex as it orbits and merges with the vortex from the outer edge of the right inboard flap. Also shown in this figure is the resulting trajectory for an angle of attack of 8° with gear down. At a 5.8° angle of attack the effect of the landing gear on the trajectory begins to appear in the third quadrant as an acceleration of the inward spiral of the wing tip vortex. This suggests that the presence of the gear results in preserving concentrated vorticity at the outboard edge of the flap; and is probably associated with a weakening of the inner edge vortex due to its proximity to the turbulence generated by the gear. At the higher angle of attack the tip vortex is at a greater distance from the flap vortex as it swings up and

inboard; but at 180° it is at a distance comparable to that of the 5.8° angle of attack. As it rotates through the third quadrant it – like the low angle of attack gear-down configuration – accelerates its inward spiral toward merging with the flap vortex.

At an 8° angle of attack the wing tip vortex orbits about the flap vortex at a faster rate and merges with it sooner than at the lower angle of attack. This is illustrated in figures 24 through 26, where the 8° data is compared with faired lines representing the 5.8° angle of attack data of figures 20 through 22. The tip vortex is: (1) further away from the flap vortex when directly above it (fig. 25), (2) arrives at the 180° position a span sooner, (3) reaches the 270° position two spans sooner, and (4) orbits into the fifth quadrant before merging at comparable downstream distances as the 5.8° data. The increased angular rate of motion of the tip vortices at an 8° angle of attack results in their separation distance decreasing more rapidly to the minimum separation at 180° of rotation and then increasing sooner than the 5.8° data (fig. 26). However, the minimum separation distance is comparable to that at the lower angle of attack. After tip flap vortex merging at this higher angle of attack with gear down, the resulting two diffuse clouds eventually reformed into two well-defined vortices again.

When this configuration was tested at an angle of attack of 2.9° with the gear up, the flap and tip vortices did not merge and the wing tip vortices persisted. The horizontal tail vortices merged with the outer edge flap vortices and both were dissipated before the very slow-moving wing tip vortices moved inboard and down. Both the horizontal tail vortex and the wing and flap vortices' relative strengths and speeds appear to play prominent roles in the dynamics of the vortex system.

All of the data discussed above with respect to the *LDG/O* configuration was obtained from film strips and photographs of light sheet runs. Similar conclusions can be reached from the streaming dye photos with the following exceptions: (1) with gear up, the tip vortex appears to merge with the flap vortex after only 180° of rotation, (2) with gear down, the tip vortex appears to merge with the flap vortex at 270°, but the flap vortex appears to persist after merging. These apparent differences may be the result of differences in lighting between the two types of flow visualization techniques. The dye sheet photos should yield the more exact results.

The effect of horizontal tail incidence was investigated for the *LDG/O* gear-up configuration. The tail incidence was varied from +4° to −4°, without any noticeable changes in the trajectories or merging characteristics of the flap and wing tip vortices. However, at a model angle of attack of 5.8° the trajectories of the horizontal tail vortex were different for each incidence tested. At +4° incidence (leading edge up 4°) the tail vortex had a downward slope of 10°. It was tightly wound, straight, and as it passed between the flap vortices prior to merging, it became diffuse. At zero incidence (at which all of the other data of this test were taken) the tail vortex downward slope increased to 15°. It was again tightly wound and straight, but became sinusoidal as it approached the flap vortices. During merger it swirled up around the outside of the vortex from the outer edge of the flap. At −4° incidence the vortex sloped downward at a 20° angle. It was diffuse, although straight, and lost most of its visual structure as it approached the flap vortices. There were faint signs of swirl during merger with the flap. In all cases the vortex from the tail moved downward and merged with the flap vortices. The angle of attack of the horizontal tail α_t, is modified by the downwash from the wing ϵ, and any incidence between the wing i_w, and the horizontal tail i_t,

$$\alpha_t = \alpha_w - \epsilon + i_t - i_w$$

For the *LDG/O* configuration at an angle of attack of 5.8°, 63 percent of the wing lift is developed over the inboard 40 percent of the semispan in the region of the inboard flap (fig. 19). As a result, the downwash angle in the vicinity of the tail is estimated to be in the neighborhood of 7°. The wing incidence varies from 2° at the wing root to −2° at the wing tip. Assuming a value of 1° over the inboard 40 percent of the wing yields the following approximation for angle of attack of the tail (for an angle of attack of 5.8°):

$$\alpha_t \simeq i_t - 2$$

Hence, for all tail incidences less than 2° the tail should be lifting downward and the tail vortices would be expected to move up away from the model. The tendency for the vortex to rise should increase as the tail incidence becomes more negative. However, just the opposite was found, i.e., the tail vortices always moved downward into the flap vortices, and the lower the tail incidence angle, the steeper the angle at which the tail vortex descended. Their descent is probably associated with the induced downward component of velocity in their flow field created by the flap vortices rotational velocities. But why the descent is steeper for the lower tail incidence angles is not clear.

Recent flight tests (ref. 5) of a 747 in the *LDG/O* (gear-up) configuration have indicated that the effect of 5° of yaw on the wake reduces the vortex alleviation of the lee side vortex. As a result of this conclusion, the water tank model was tested in the *LDG/O* configuration with 5° of yaw at an angle of attack of 5.8°. No asymmetries due to yaw were noticed in the wake. Perhaps the asymmetries in the flight results were a result of control deflections to maintain level flight.

MOD LDG/O Configuration

In an attempt to eliminate the gear effect on the wake alleviation capability of the *LDG/O* configuration, 30 percent of the inboard span of the flap was removed. This configuration was designated *MOD LDG/O*. The purpose was to move the vortex from the inboard edge of the flap to closer proximity with the stronger outboard edge vortex. The result would be a rotation of the inboard vortex away from the region of the fuselage and turbulence associated with the landing gear. The predicted span load distribution for this configuration at a 5.8° angle of attack is shown in figure 27. A comparison with figure 19 shows a predicted life coefficient loss of 12 percent associated with the reduced flap span. The load gradient at the inboard side of the flap has been steepened, suggesting that the net result on the flap vortex pair might be to swing down and out as the inboard vortex rotates below the outboard vortex.

The flow visualization indicated an inner edge flap vortex much less diffuse than it was in the *LDG/O* configuration, and that immediately after formation it began to rotate below the outer edge flap vortex. At just over one span downstream, the tail vortex began to merge with the flap outer edge vortex; two spans later they were completely merged and the inner edge vortex was directly below the outer edge vortex. The tail vortex appeared to move down along the outboard side of the outer edge flap vortex and wrap around it. An elongation of the flap doublet resulted from the tail merging. The outboard edge flap vortices began to drift down and outboard immediaely after formation. Figure 28 presents a comparison of the separation distance between outboard edge flap vortices as a function of downstream distance for the *MOD LDG/O* and *LDG/O* configurations. It is seen that the outer edge flap vortex moves outboard at a greater rate and to a greater distance for the modified configuration. As the flap doublets moved apart, their vortices became more diffuse

and elongated. By ten spans – when the wing tip vortices are passing between the flap doublets (at 180°) – it is not possible to identify individual flap vortices.

The wing tip vortices moved up and inboard and then down between the flap doublets. They never merged with the outward moving, diffuse, flap vortices. A comparison of the separation distance between the wing tip vortices as a function of downstream distance for the *MOD LDG/O* and *LDG/O* configurations is presented in figure 29. The tip vortices move together at a slower rate for the modified configuration and after 180° of rotation about the outer edge flap vortices (at about 10 spans downstream) they remain at a constant distance from each other as they persist and slowly descend. Figure 30 illustrates their persistence and constant descent rate of 5.4 cm/sec until bottom effects are experienced at about 23 spans downstream. A comparison of trajectories of the right wing tip vortex about the right outer edge flap vortex for the *MOD LDG/O* and *LDG/O* configurations is presented in figure 31. Bringing the inboard edge flap vortex outboard 30 percent closer to the outboard edge flap vortex resulted in a span loading change which strengthened the inboard edge vortex (fig. 27). The interaction of this strengthened vortex with the outboard edge vortex, coupled with their movement downward and outward, precluded a flap/wing tip vortex merger. As a result, instead of the tip vortex following a spiral trajectory to merge with the flap (as it did in the *LDG/O* configuration) the flap vortices merge after a 180° rotation of the tip vortex and the tip vortices persist. Hence the attempt at eliminating the gear effect on the *LDG/O* configuration by a small change in flap span created a new problem. This indicates that small or subtle changes in span loading may result in large changes in wake characteristices.

MOD LDG/T.O. Configuration

In an attempt to slow the outboard movement of the flap doublet – in anticipation of a resulting flap, wing tip, vortex interaction – and to recover some of the lift coefficient lost by removing the inboard 30 percent of the inboard flap, the outboard flaps were lowered to the takeoff position. This configuration was called the *MOD LDG/T.O.* The predicted span loading at a 5.8° angle of attack is presented in figure 27. The resulting wake was basically the same as the *LDG/O* configuration, since the span loadings of these configurations are quite similar (fig. 27). However, the outboard edge vortex from the inboard flap was more diffuse, and the outboard edge vortex from the outboard flap merged with the wing tip vortex at about two spans. This merging of the flap vortex with the wing tip vortex caused the latter to elongate in cross section and induce a spiral arm in the shape of the tip vortex.

The movement outboard of the inboard flap's vortex doublet was slowed by deployment of the outboard flaps to the takeoff position. This is evident in figure 32 where the distance between outboard edge vortices from the inboard flaps are presented as a function of downstream distance for the *LDG/O, MOD LDG/O* and *MOD LDG/T.O.* configurations. Although these flap vortices stayed closer to the model centerline for the *MOD LDG/O* configuration, they were still far enough apart to allow the wing tip vortices to pass between them without merging. A comparison of the actual wing tip vortex trajectories of the three configurations presented in figure 32 is shown in figure 31. Changing from the *LDG/O* to the *MOD LDG/O* configuration brought the flap doublet closer together and appeared to weaken the inboard flap outer edge vortex. The wing tip vortex moved slower and further away from the flap vortex as it drifted upward and inboard and finally descended and persisted. Changing to the *MOD LDG/T.O.* configuration further degraded the strength of the inboard flap outer edge vortex due to its proximity to the outboard flap inboard

vortex. The wing tip vortex moved still further away from the flap vortex as it passed above; however, it was at the same distance from the flap vortex as the *MOD LDG/O* configuration after 180° rotation. This latter result suggests that the wing tip vortices were dictating the closest proximity to each other.

MOD LDG Configuration

Since the change from the *MOD LDG/O* to the *MOD LDG/T.O.* configuration slowed the outboard movement of the inboard flap doublet – although not enough to cause flap wing tip vortex merging – a decision was made to lower the outboard flaps still further to the landing position. This was called the *MOD LDG* configuration. Its predicted span loading at a 2.9° angle of attack is presented ir figure 17. The load gradient at the inboard edge of the inboard flap has been enhanced in comparison to the normal landing configuration. The wake characteristics resembled those of the landing configuration in the near-field, but did not develop into the persistent vortices associated with the landing configuration in the far-field. The wake had none of the characteristics of any of the other modified configurations.

The flap vortices were very diffuse. The outboard edge vortex off the inboard flap rotated very rapidly to a position directly below the inboard edge vortex and the doublet moved inward toward the model centerline, when at 1.3 spans it merged with the doublet from the opposite side (fig. 12). The merging resulted in a diffuse cloud with no distinguishable vortices remaining. The horizontal tail vortices moved down but were outboard of the merged flap doublets and did not merge with them. The wing tip vortices moved up and inboard, and at 3.3 spans merged with the vortices from the outboard side of the outboard flaps. The resulting vortices were the flap vortices which appeared to grow in diameter and merge with the tail vortices at eightspans. These vortices had a very low descent rate (almost half that of the conventional landing configuration) and drifted outboard from each other (fig. 33). As they drifted out and down, they became increasingly diffuse and after 18 spans downstream, they could no longer be identified as vortices but as separate, large areas of diffuse dye clouds (fig. 12).

From recorded visualization of the flow in the wake of the configurations tested and discussed above, the *MOD LDG* configuration appears to yield the wake with the least amount of concentrated vorticity, and seems to be the most attractive as a possible alleviation scheme for the conventional landing configuration.

CONCLUSIONS

A flow visualization technique has been developed and used to investigate vortex interactions in multiple vortex wakes. Different wake characteristics were generated by changing both the attitude and flap geometry of a 0.01 scale model of a 747 transport. The following results were obtained:

1. Visualization of the wakes of seven different configurations of the model has established that the behavior of these wakes are sensitive to small changes in wing span loading or model attitude. Realistic span loadings were achieved which resulted in multiple vortex interactions and merges within the wake and yielded diffuse, slowly rotating wakes. Removing the inboard 30 percent of the span of the inboard flaps of the landing configuration changed the wake from being characterized by two persistent, highly concentrated vortices to a wake which appeared to dissipate

and contain minimal vorticity by 18 spans downstream. Changes in model angle of attack for a given configuration showed that both the relative strengths and speeds of motion of the vortices in a multiple vortex wake play important roles in characterizing the final wake.

2. In concurrence with recent flight tests of a 747, it was found that the landing gear deployment caused a far-field reconcentration of vorticity behind a model configuration which dissipated near-field concentrated wake vorticity.

3. In general, vortices that remain isolated in a multiple vortex wake – in the absence of external disturbances – tend to persist. Alleviation of wake vorticity is attained by causing the wake vortices to interact and merge.

4. The vortices shed from the horizontal stabilizer always moved down into the wake and merged with other vortices: primarily the inboard flap vortices. Although the tail was lifting downward for most of the configurations tested, the local induced velocity field forced its wake downward. When they merged with the flap vortices distortions or elongations were usually caused in the dye pattern of the flap vortices. The tail vortices seem to play a significant role in vortex interactions within the wake; however, their ultimate effect on the wake must be quantitatively ascertained.

5. When the model was yawed 5° with its inboard flaps in the landing position and outboard flaps retracted, there were no obvious asymmetries visible in the wake. The effects of yaw seen in flight may have been a consequence of control deflections required to maintain flight attitude equilibrium.

6. Most of the configurations tested had vortex interactions and merging completed by 13 spans downstream. Hence, the vortex merging phenomena could be investigated in the Ames 40- by 80-Foot Wind Tunnel (ref. 4). Since most of the vortex merging involving the horizontal tail vortices was completed by three spans, the details of these interactions could be studied in the Ames 7- by 10-Foot Wind Tunnel (ref. 11).

7. When the wake contains only a vortex pair (i.e., when a pair is isolated and does not merge with other vortices, or a pair results from multiple vortex merging), their decay characteristics should be predictable from available empirical correlations (ref. 12).

8. The water tow facility has proven to be an extremely useful tool in investigating the wake characteristics behind aircraft models, particularly in the far-field, a region of interest that is not explorable in wind tunnels. Far-field wake characteristics that were suggested from flight tests (ref. 5) have been verified in the water tow facility.

REFERENCES

1. Rossow, V. J.: On the Inviscid Rolled-up Structure of Lift-Generated Vortices. Journal of Aircraft, vol. 10, no. 11, Nov. 1973, pp. 647-650.

2. Rossow, V. J.: Theoretical Study of Lift-Generated Vortex Wakes Designed to Avoid Rollup. AIAA Journal, vol. 13, no. 4, April 1975, pp. 476-484.

3. Ciffone, D. L.; and Orloff, K. L.: Far-Field Wake-Vortex Characteristics of Wings. Journal of Aircraft, vol. 12, no. 5, May 1975.

4. Corsiglia, V. R.; Rossow, V. J.; and Ciffone, D. L.: Experimental Study of the Effect of Span Loading on Aircraft Wakes. AIAA 8th Fluid and Plasma Dynamics Conference, Hartford, Conn., June 1975, NASA TMX-62,431, May 1975.

5. Tymczyszyn, J.; and Barber, M. R.: A Review of Recent Wake Vortex Flight Tests. 18th Annual Symposium of Society of Experimental Test Pilots, Los Angeles, Calif., Sept. 26, 1974.

6. Orloff, K. L.; Ciffone, D. L.; and Lorincz, D.: Airfoil Wake Vortex Characteristics in the Far Field. NASA TMX-62,318, Nov. 1973.

7. Kirkman, K. L.; Brown, C. E.; and Goodman, A.: Evaluation of Effectiveness of Various Devices for Attenuation of Trailing Vortices Based on Model Test in a Large Towing Basin. NASA CR-2202, December 1973.

8. Wadlin, K. L.; Ramsen, J. A.; and McGehee, J. R.: Tank Tests at Subcavitation Speeds of an Aspect Ratio-10 Hydrofoil with a Single Strut. NACA RM L9K14a, July 1950.

9. Hough, G.: Remarks on Vortex-Lattice Methods. AIAA Journal of Aircraft, vol. 10, no. 5, May 1973, pp. 314-317.

10. Crow, S. C.: Stability Theory for a Pair of Trailing Vortices. AIAA Journal, vol. 8, no. 12, Dec. 1970, pp. 2172-2179.

11. Ciffone, D. L.; Orloff, K. L.; and Grant, G. R.: Laser Doppler Velocimeter Investigation of Trailing Vortices Behind a Semi-Span Swept Wing in a Landing Configuration. NASA TMX-62,294, Aug. 1973.

12. Ciffone, D. L.: Correlation for Estimating Vortex Rotational Velocity Downstream Dependence. AIAA Journal of Aircraft, vol. 11, no. 11, Nov. 1974, pp. 716-717.

TABLE 1.- PRINCIPAL GEOMETRIC CHARACTERISTICS OF 747 MODEL

Scale	0.01 full scale
Wing cm (in.)	
Span	61.0 (24.0)
Root incidence	2.0 deg
Tip incidence	−2.0 deg
Mean aerodynamic chord	8.71 (3.43)
Root chord	16.7 (6.57)
Tip chord	4.06 (1.6)
Sweepback (at 1/4 chord)	37.5 deg
Area, cm^2 (ft^2)	536. (0.578)
Aspect ratio	6.96
Fuselage cm (in.)	
Length	70.2 (27.6)
Horizontal Stabilizer cm (in.)	
Span	22.6 (8.9)
Area, cm^2 (ft^2)	143. (0.154)
Aspect ratio	3.6

TABLE 2.- TEST SCHEDULE AND FILM COVERAGE

			Film coverage					
			Trailing vortices				Light sheet	
			16 mm			35 mm	16 mm	35 mm
Configuration	U_∞	α (deg)	Under-water	Side (near)	Side (far)	Side (Slides)	Under water	Side (prints)
Take off, G	1	5.8		119			C1(119)	C1(119)
		8.0		121	121		D1(120)	D1(120)
Clean (Slats on)	1	29		81	81			
	2		56	80	80			
	1	5.8		79	79			
	2		54,55	75,76,77 78	75,76 77,78	75*,76*		
	1	10°		83	83			
	2		52,53	82	82			
LDG	1	2.9	36,37,39			37		
	2		34,35,38					
LDG,G	1	2.9	51	103,115 117,118	103		B1(117) cc(115)	B1(117) 103**
	2		49,50	104	104			
LDG/O°	1	8.0	1,2,5,6,7, 8,9,10,11 12	69,73,84 85	69,73,84 85	73*		
	2		3,23,24, 25,26	70,71,72 74,86,87	70,71,72 74,86,87	87,72* 70*,71* 74*		
	1/2		4					
	1	2.9	13,14,15	94,95	94,95			
	1	5.8		88,89 113	88,89		AA(113)	AA(113)
	2			90	90	90		

TABLE 2.- TEST SCHEDULE AND FILM COVERAGE – Concluded

			Film coverage					
			Trailing vortices				Light sheet	
			16 mm			35 mm	16 mm	35 mm
Configuration	U_∞	α (deg)	Under-water	Side (near)	Side (far)	Side (slides)	Under water	Side (prints)
LDG/O°,G	1	8.0	31,32	101,102 116	102		A1(116)	A1(116)
	2		29,30	98,99,100	98,99,100	101+		
	1	5.8		114			BB(114)	BB(114),F'**,G'**
LDG/O°, 5° yaw	1	5.8	61,62	97	97			
	2		63,64	96	96	97+		
LDG/O° $\delta_t = -4°$	1	5.8	59,60	92	92			
	2		19,20	91	91	91		
	2	8	21,22					
LDG/O° $\delta_t = 4$	2	8	27,28					
		5.8		93	93	93		
MOD LDG	1	2.9	42,43,44	107	107	43,43+,44 44+		
	2		40,41,45	108	108			
MOD LDG,G	1	2.9	48	105,125	105		H1(125)	H1(125)
	2		46,47	106	106			
MOD LDG/O°,G	1	5.8		124	124		G1(124)	G1(124)
		8		123	123		F1(123)	F1(123)
MOD I.B./T.O. O.B.	1	5.8	65,66,67 68	109,111	109			D(109)**
	2			110,112	110			
MOD I.B./T.O.O.B,G	1	5.8		122			E1(122)	E1(122)

* Prints
**Slides

TABLE 3.- SUMMARY OF PERTINENT CAMERA DATA

16-mm Side camera (far) (trailing vortices) (DBM) (lens 10 mm) (shutter 160°) (7242 film)				
Run numbers	Date	F Stop	F.P.S.	Comments
69,70,71	3-13-75	1.8	250	
72-76	3-13-75	↓	100	
77-81	3-17-75	↓	↓	
82-91	3-17-75	↓	↓	
92-100	3-17-75	↓	↓	
102-108	3-17-75	↓	↓	
109-110,121,123-124	3-19-75	↓	↓	
16-mm Side camera (near) (trailing vortices) (DBM) (lens 25 mm) (shutter 160°) (7242 film)				
Run numbers	Date	F Stop	F.P.S.	Comments
69,70,71	3-13-75	1.4	128	
72-76	3-13-75	↓	↓	
77-80	3-17-75	↓	↓	
81-83	3-17-75	↓	↓	
84-88	3-17-75	↓	↓	
89-94	3-17-75	↓	↓	
95-100	3-17-75	↓	↓	
101-105	3-17-75	↓	↓	
106-110	3-19-75	↓	↓	
111-115	3-20-75	2.0	↓	
116-119	3-21-75	2.8	↓	
121-124	3-21-75	↓	↓	
125	3-21-75	↓	↓	
16-mm Underwater camera (trailing vortices) (DBM) (lens 10 mm) (shutter 160°) (7242 film)				
Run numbers	Date	F Stop	F.P.S.	Comments
1-5	3-5-75	1.8	100	
6-12	3-5-75	↓	↓	
13-15	3-6-75	↓	↓	
19-24	3-6-75	↓	↓	
25-33	3-6-75	↓	↓	
34-39	3-7-75	↓	↓	

TABLE 3.- SUMMARY OF PERTINENT CAMERA DATA – Continued

16-mm Underwater camera (trailing vortices) – Continued

Run numbers	Date	F Stop	F.P.S.	Comments
40-45	3-7-75	1.8	100	
46-51	3-10-75	↓	↓	
52-58	3-10-75			
59-64	3-11-75			
65-68	3-11-75			

16-mm Underwater camera (dye sheet) (DBM) (lens 10 mm) (shutter 160°) (7242 film)

Run numbers	Date	F Stop	F.P.S.	Comments
A,B,C,D,E	3-19-75	2.8	64	
AA-EE	3-20-75	1.8	↓	Pushed 1 stop
A1,B1,C1,D1,F1	3-21-75	↓		Pushed 2 stops
G1,H1	3-21-75			Pushed 2 stops

35-mm (SLR camera) trailing vortices, EFB (7242 film)

Run numbers	Date	F Stop	F.P.S.	Slides	Prints	Comments
37	3-7-75		2.5	X		from above
43	3-7-75		↓	X		
43+	3-7-75			X		
44	3-7-75			X		
44+	3-7-75			X		from above
70	3-13-75				X	
71	3-13-75				X	
72	3-13-75				X	
73	3-13-75				X	
74	3-13-75				X	
75	3-13-75				X	
76	3-13-75				X	
87	3-17-75			X		
88	3-17-75			X		
90	3-17-75			X		
91	3-17-75			X		
93	3-17-75			X		
97+	3-17-75			X		
101+	3-17-75		↓	X		

TABLE 3.- SUMMARY OF PERTINENT CAMERA DATA - Concluded

35-mm (SLR camera) dye sheet, EFB (7242 film)

Run numbers	Date	F Stop	F.P.S.	Slides	Prints	Comments
103	3-19-75	1.4	2.5	X		
F[1]	3-19-75	2.6	3	X		
G[1]	3-19-75	2.0	4	X		
D(109)	3-19-75	2.8	2.5	X		
AA(113)	3-20-75	1.4	4		X	
BB(114)	3-20-75	↓	4		X	
A1(116)	3-21-75		2.5		X	
B1(117)	3-21-75		↓		X	
C1(119)	3-21-75				X	
D1(120)	3-21-75				X	
E1(122)	3-21-75				X	
F1(123)	3-21-75				X	
G1(124)	3-21-75				X	
H1(125)	3-21-75	↓	↓		X	

TABLE 4.- CONFIGURATIONS AND ANGLES OF ATTACK INVESTIGATED

Configuration Tested	*GU*	*GD*	$\alpha = 2.9°$		$\alpha = 5.8°$		$\alpha = 8.0°$		$\alpha = 10°$	
			C_{L_T}	C_{L_E}	C_{L_T}	C_{L_E}	C_{L_T}	C_{L_E}	C_{L_T}	C_{L_E}
Clean	X			0.29	0.53	0.48			0.81	0.71
Take off		X			.57	.59	0.71	0.78		
Landing	X	X	1.09	1.20						
LDG/O	X	X	.81	.79	.92	1.07	1.10	1.23		
LDG/O, $\alpha i_t = \pm 4°$	X				X		X			
LDG/O, $\psi = 5°$	X				X					
MOD LDG/O		X			.81					
MOD LDG/T.O.	X	X			.82					
MOD LDG	X	X	.90							

☆ GPO 694-650

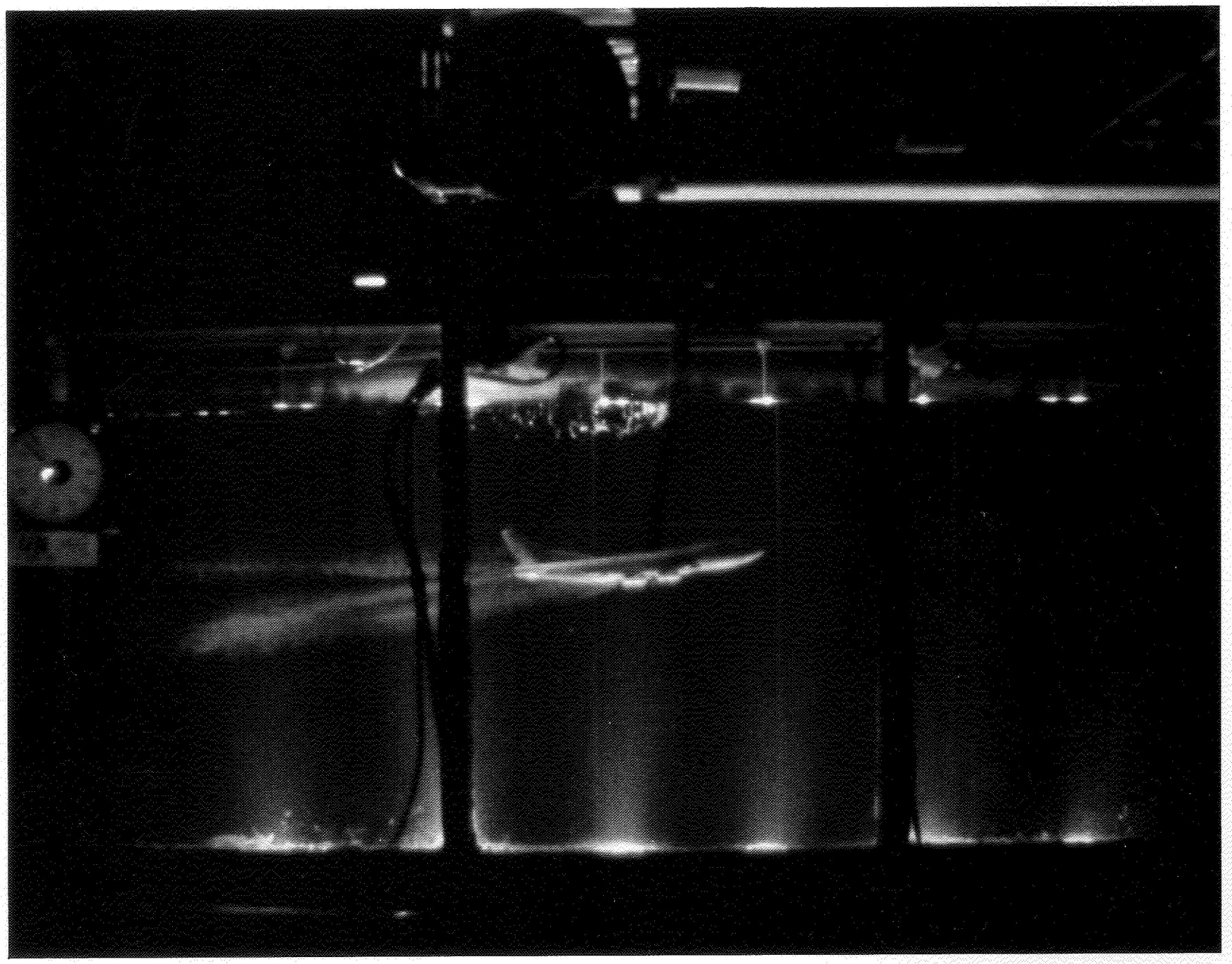

Figure 1.– Model being towed past viewing station during test.

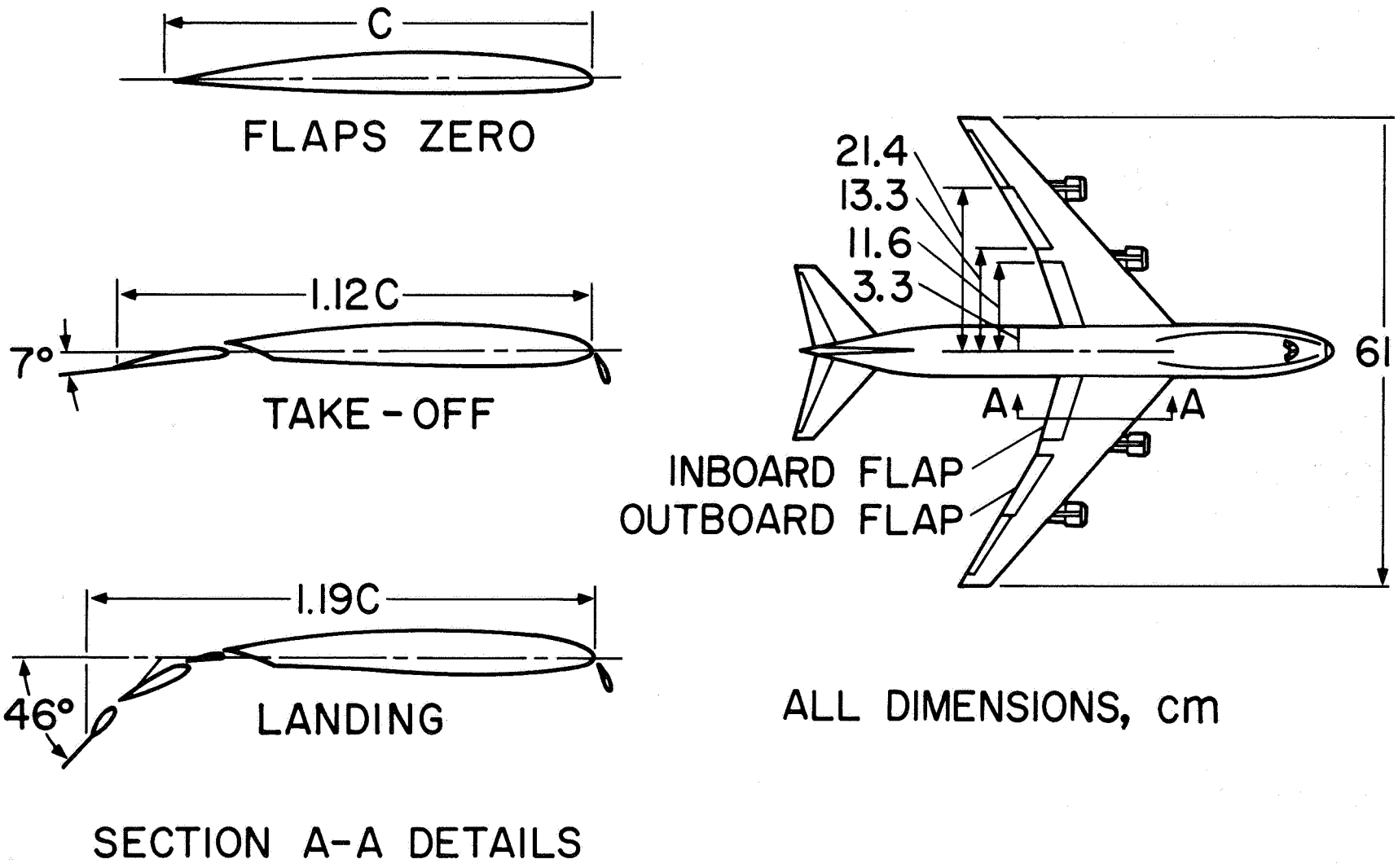

Figure 2.– 0.01 scale model of Boeing 747 Airplane.

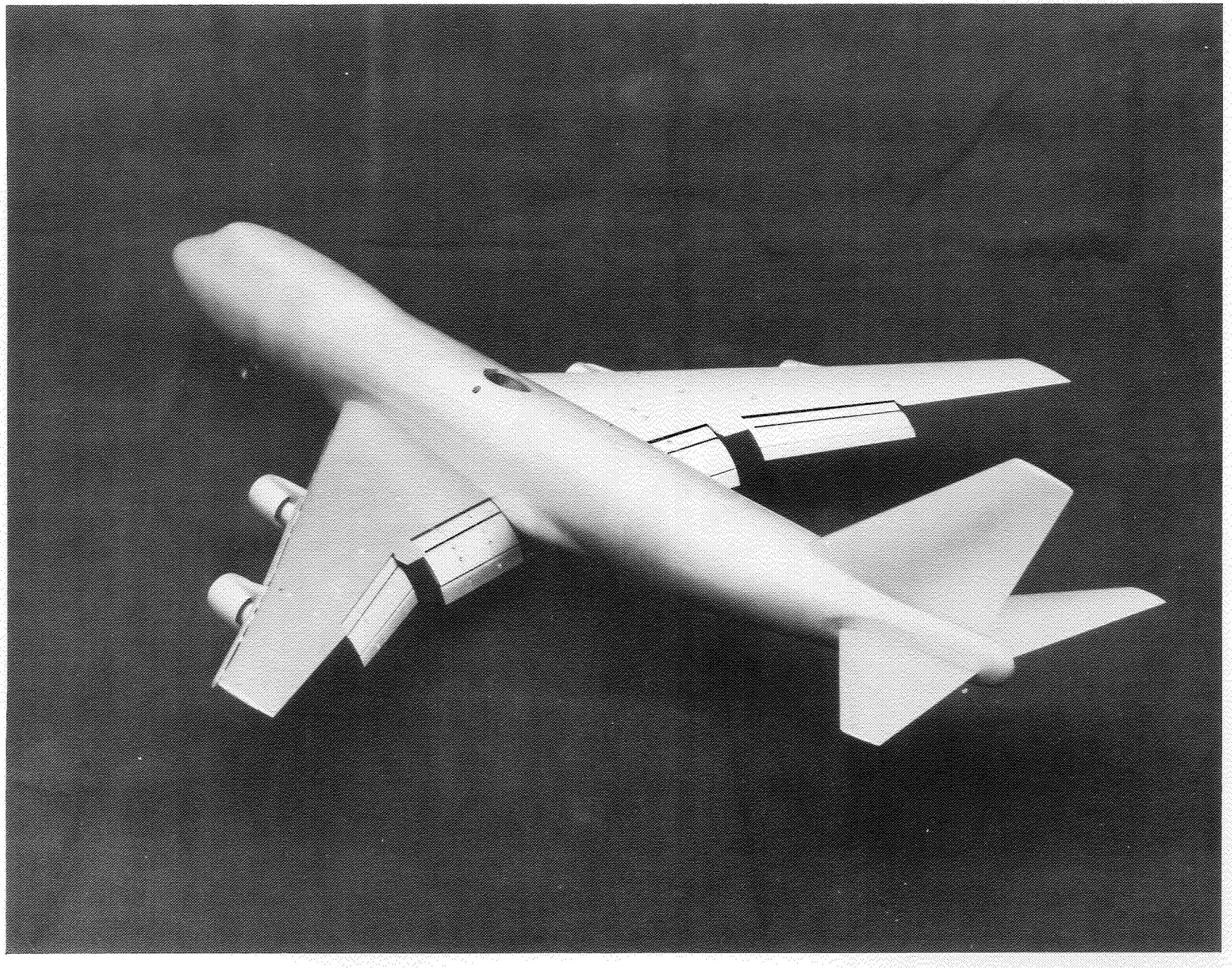

Figure 3.– Photograph of model in landing configuration; viewed from above and aft.

Figure 4.– Photograph of model in landing configuration; viewed from below and aft.

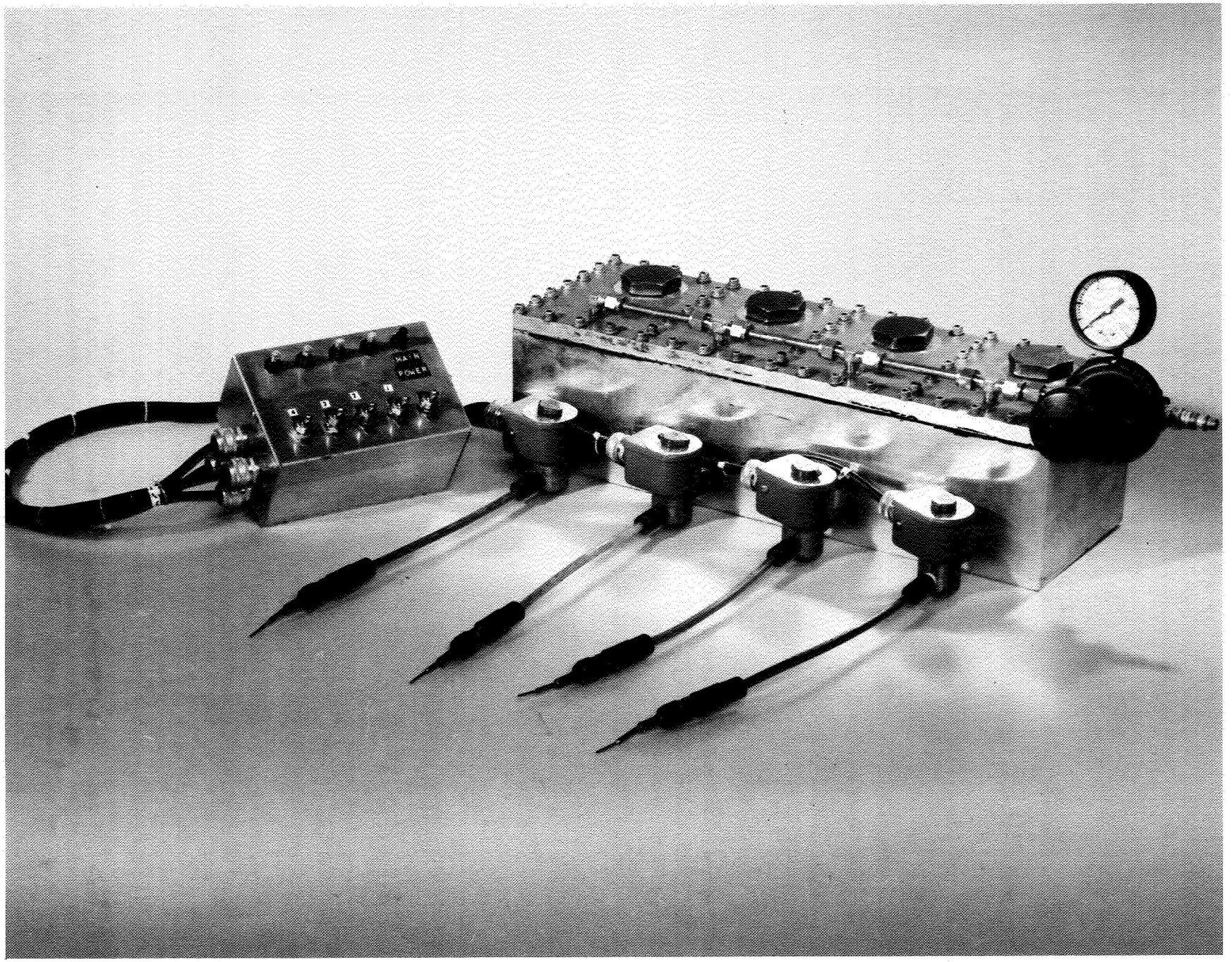

Figure 5.– Dye reservoir and ejection system.

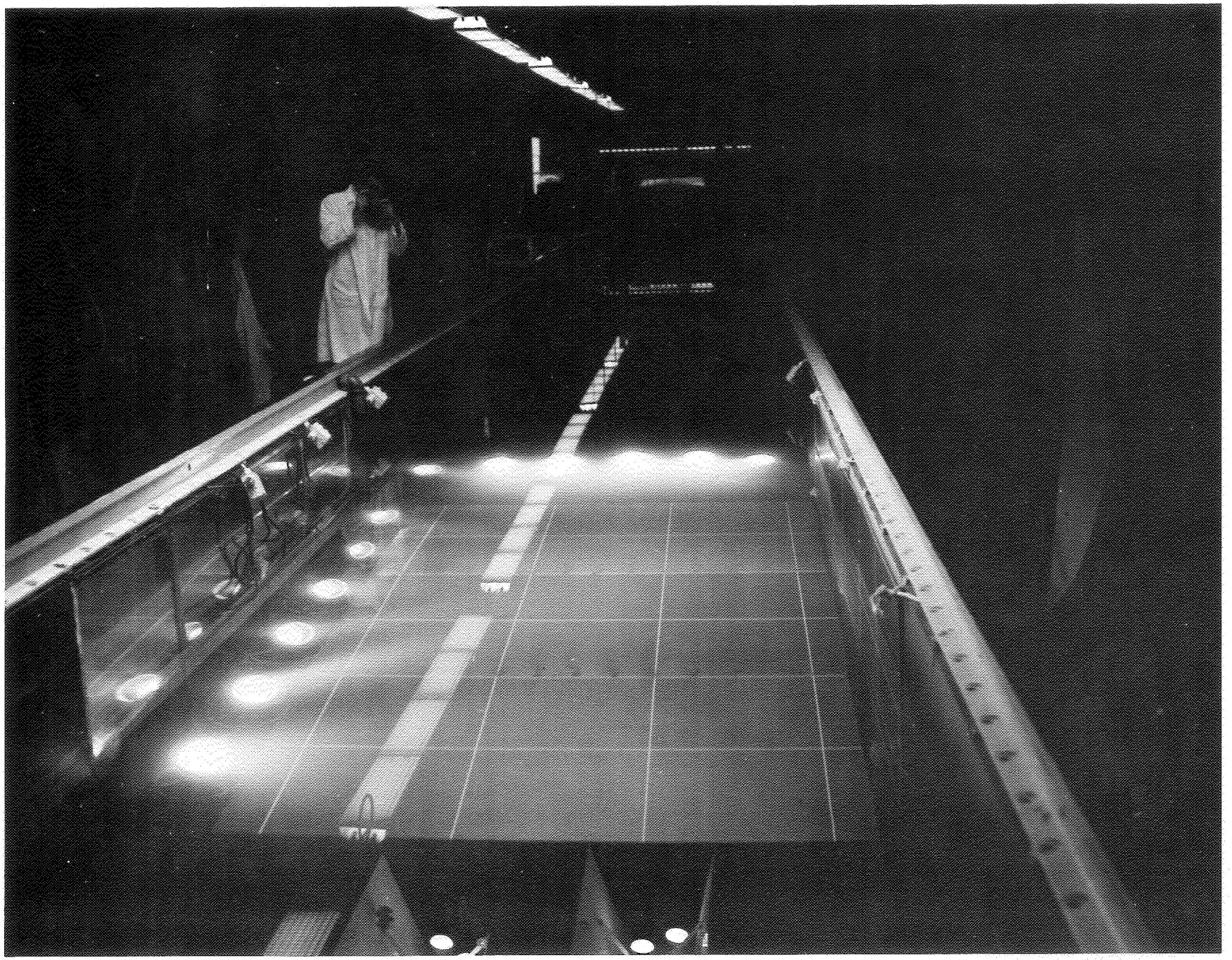

Figure 6.– Water tow-tank viewing station.

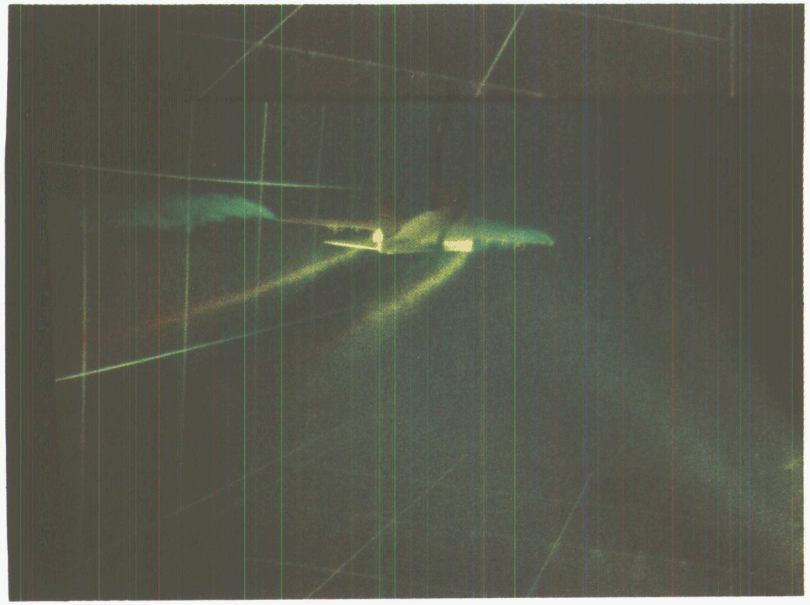

$X/b = 1.5$

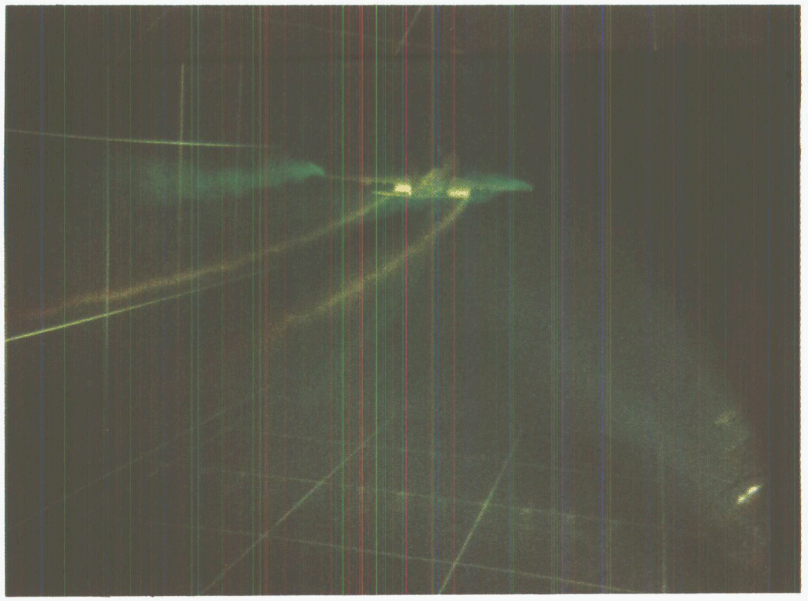

$X/b = 2.2$

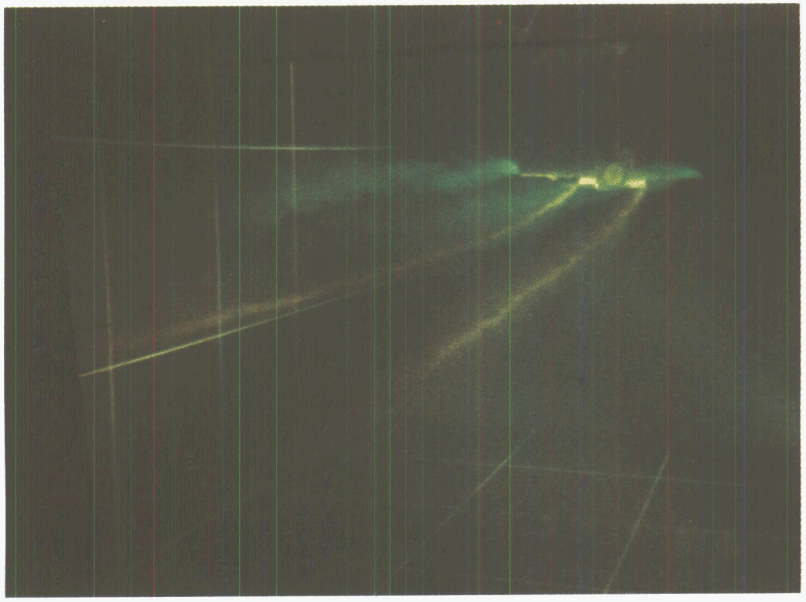

$X/b = 3.5$

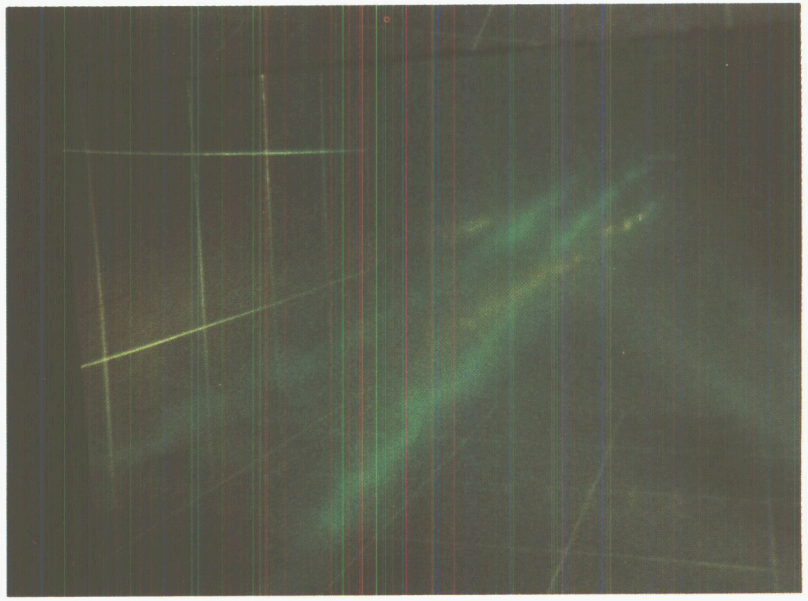

$X/b = 9.9$

Figure 7.– Underwater view of streaming vortices; LDG/O configuration, $\alpha = 8°$, $C_L = 1.2$.

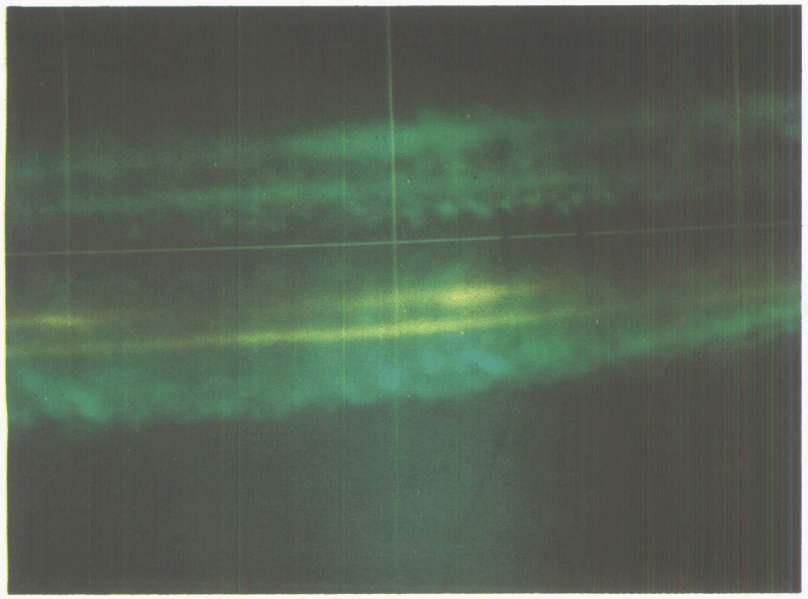

$X/b = 2.2$

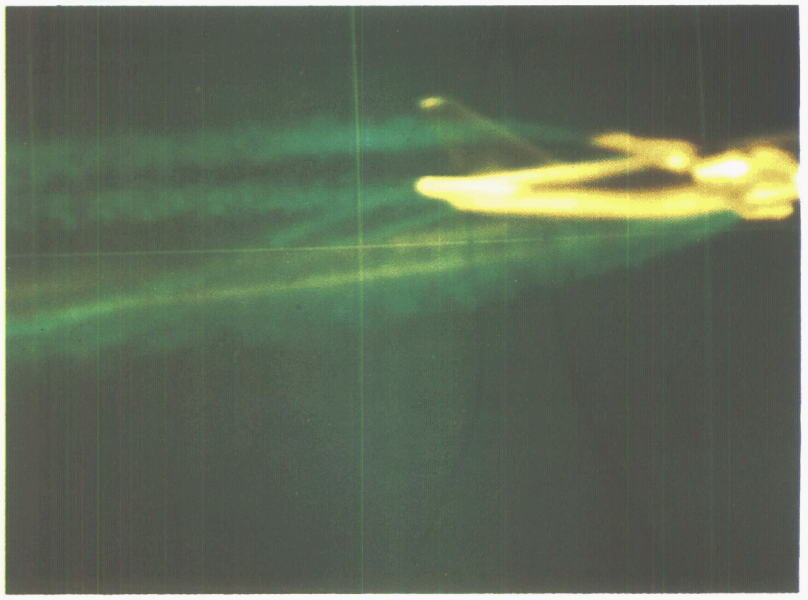

$X/b = 1.5$

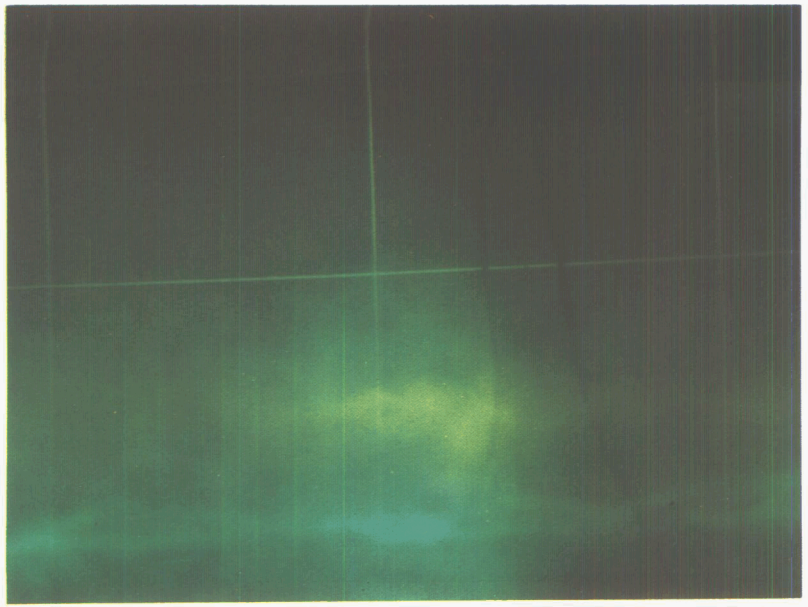

$X/b = 9.9$

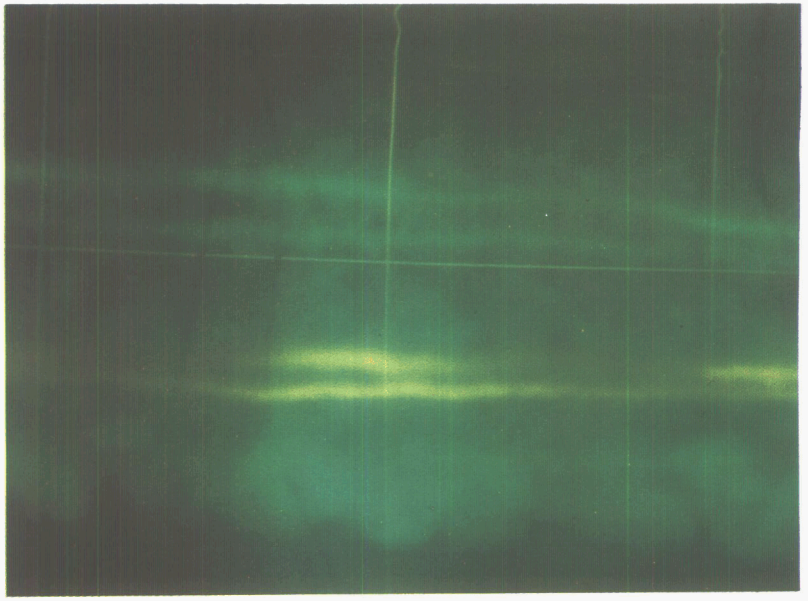

$X/b = 3.5$

Figure 8.– Side view of streaming vortices; LDG/O configuration, $\alpha = 5.8°$, $C_L = 1.1$.

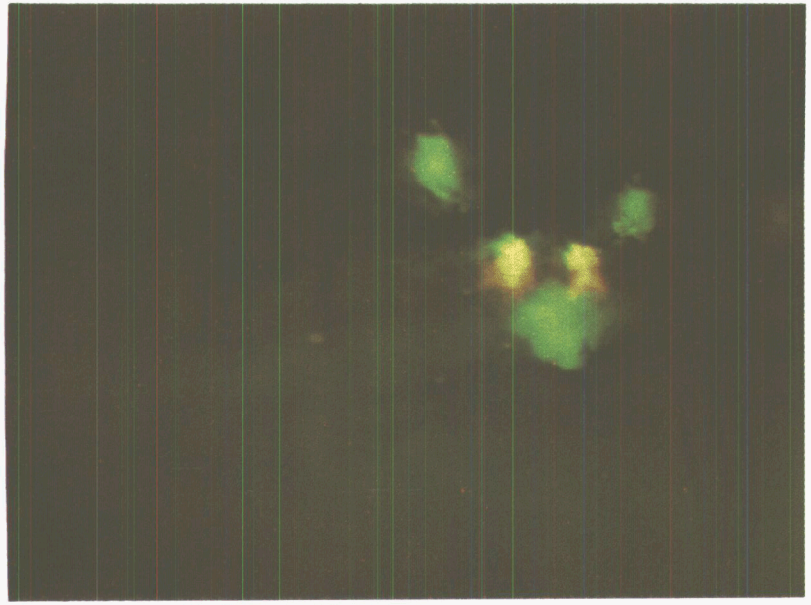

$X/b = 1.3$

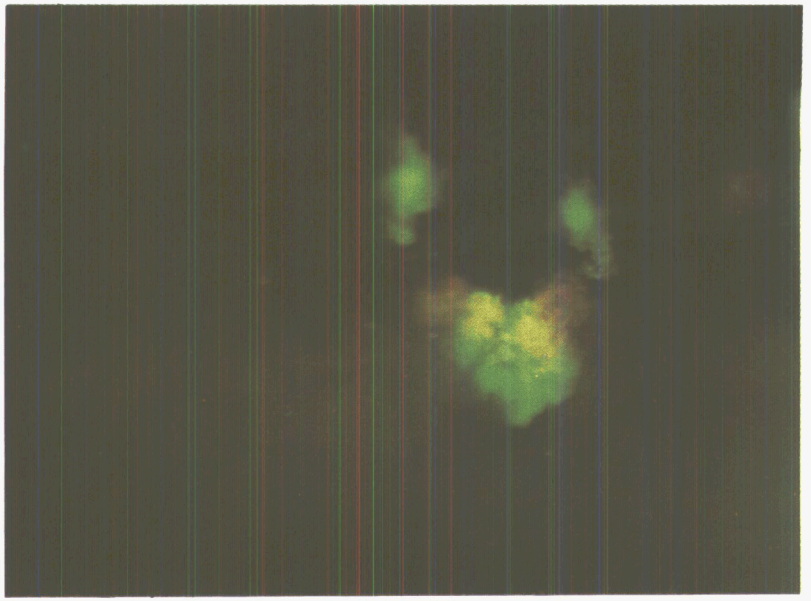

$X/b = 3.3$

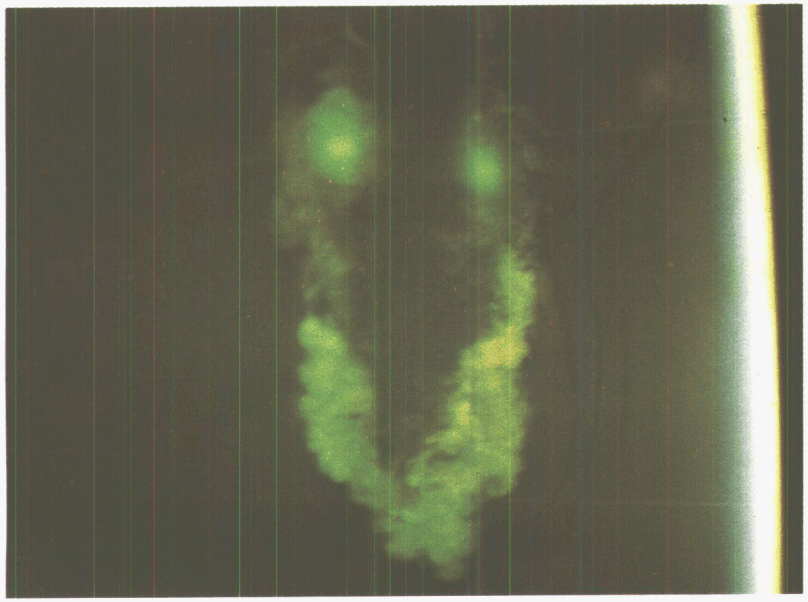

$X/b = 11.2$

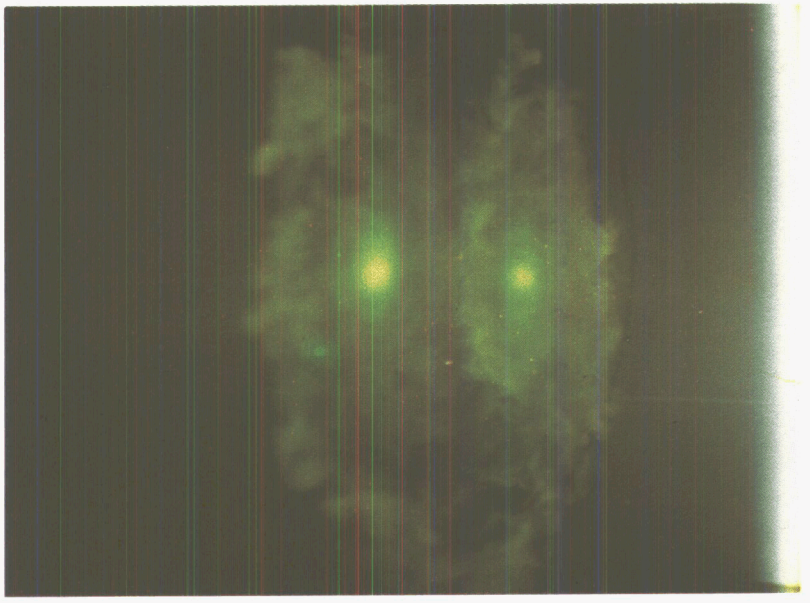

$X/b = 26.2$

Figure 9.– Cross-section through wake; take-off configuration, $\alpha = 5.8°$ $C_L = .59$, gear down.

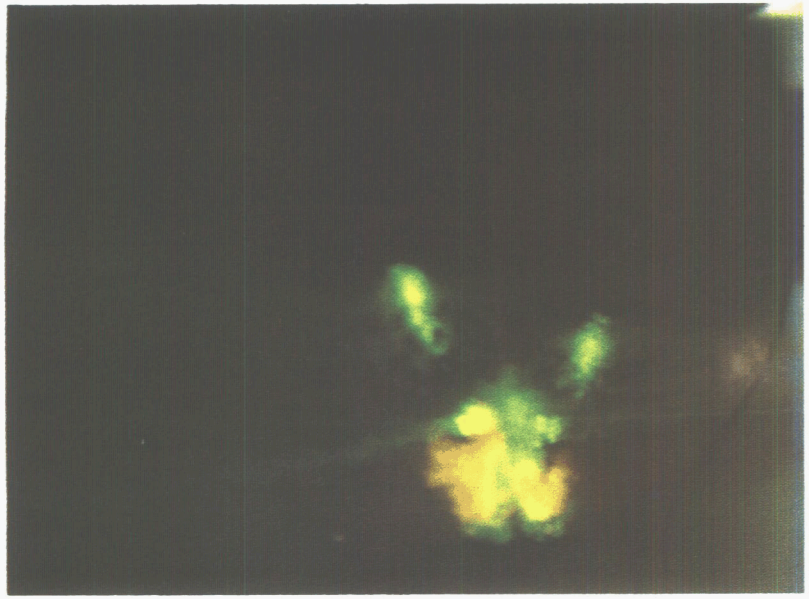

$X/b = 1.3$

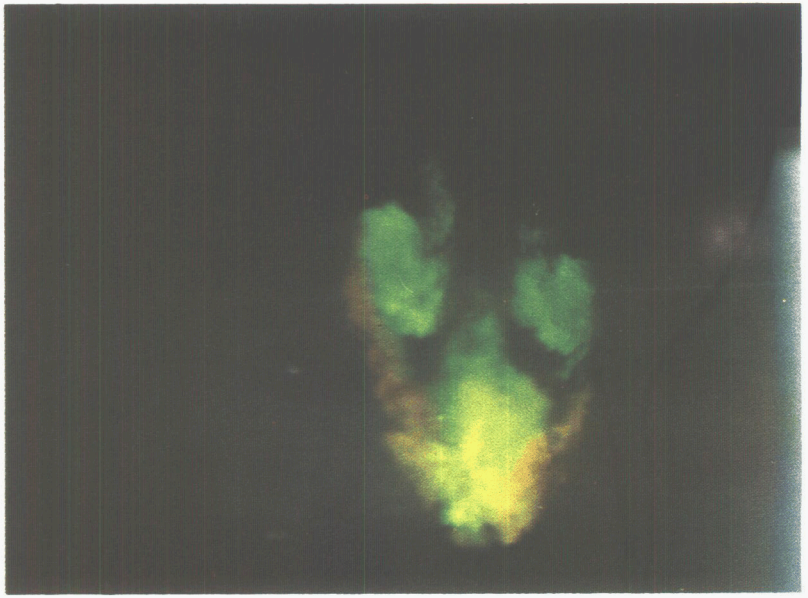

$X/b = 3.3$

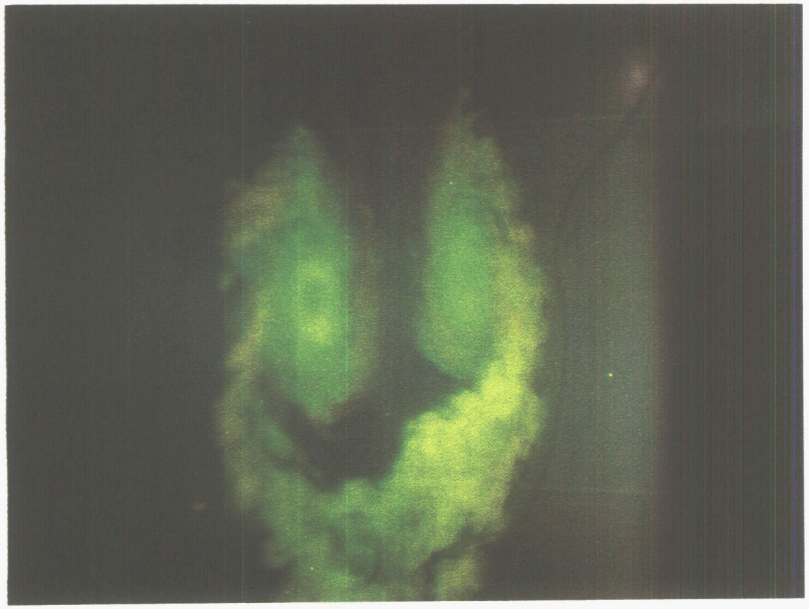

$X/b = 11.2$

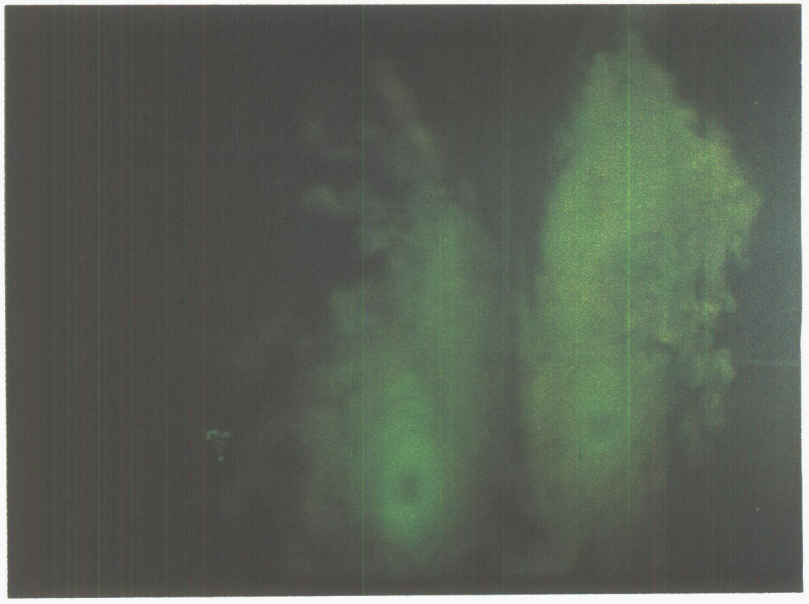

$X/b = 26.2$

Figure 10.– Cross-section through wake; landing configuration, $\alpha = 2.9°$, $C_L = 1.2$, gear down.

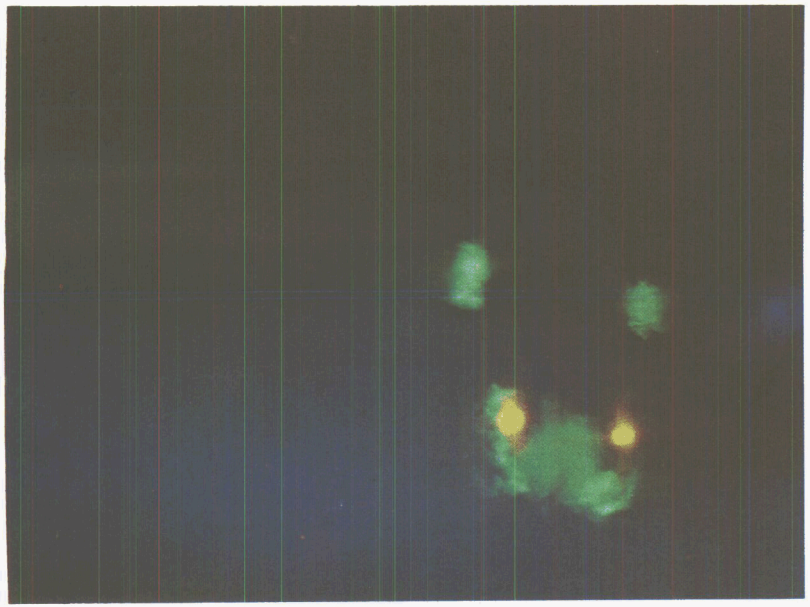

$X/b = 1.3$

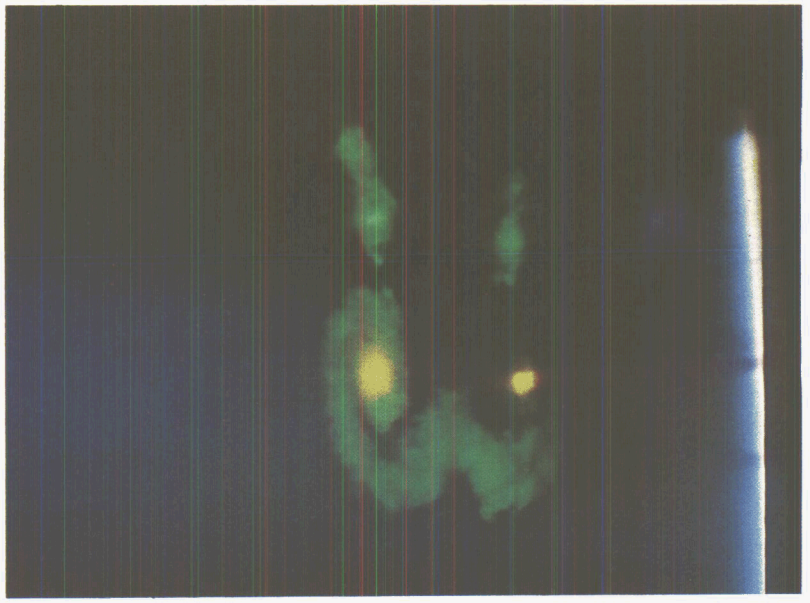

$X/b = 3.3$

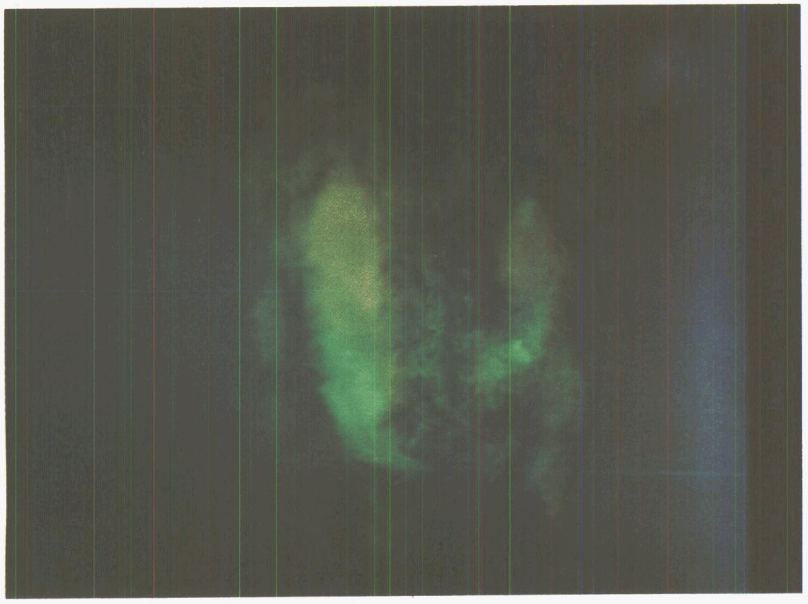

$X/b = 11.2$

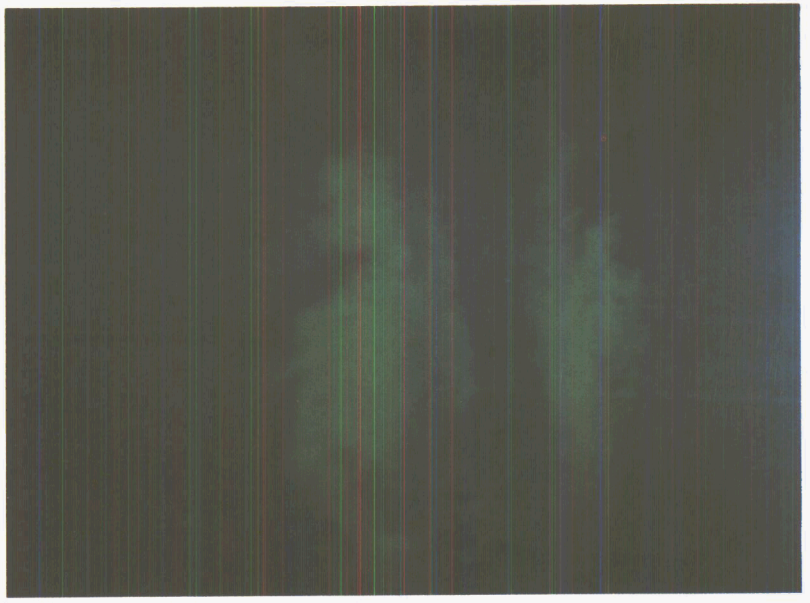

$X/b = 26.2$

Figure 11.– Cross-section through wake; LDG/O configuration, $\alpha = 5.8°$, $C_L = 1.1$, gear down.

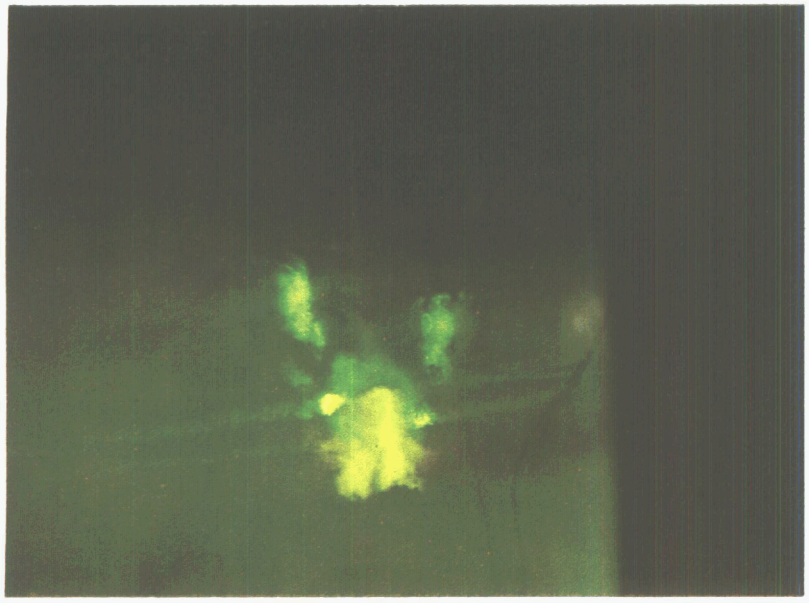

$X/b = 1.3$

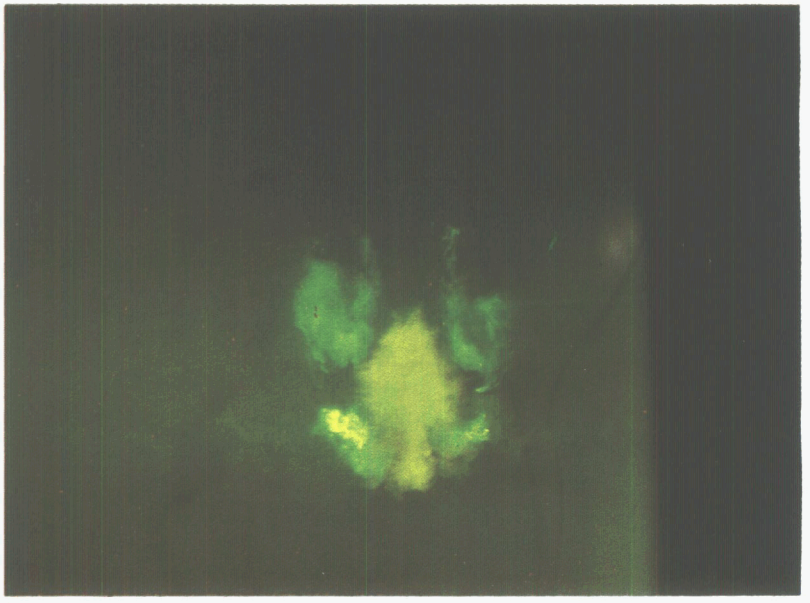

$X/b = 3.3$

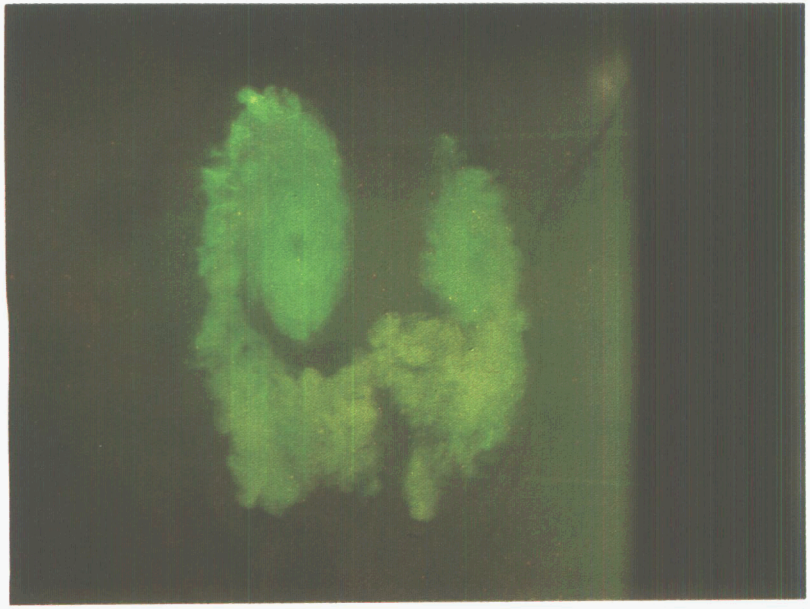

$X/b = 11.2$

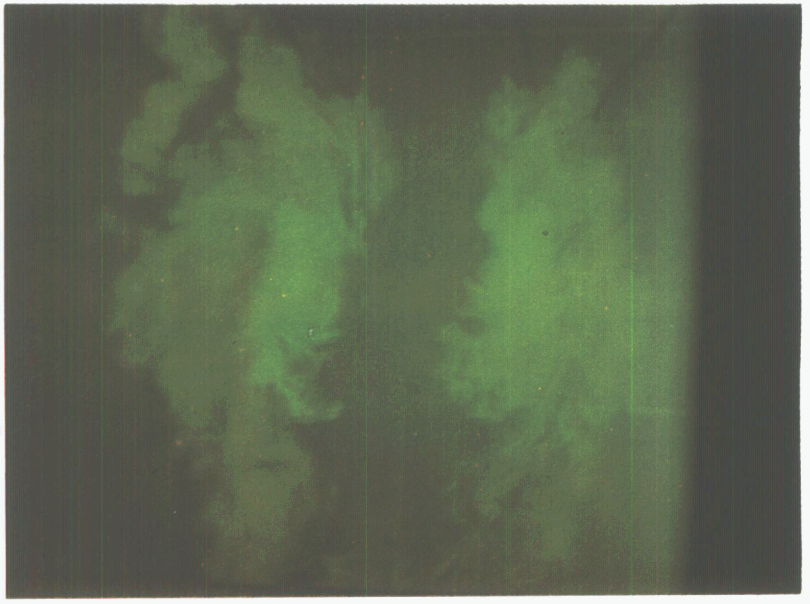

$X/b = 26.2$

Figure 12.– Cross-section through wake; MOD LDG configuration, $\alpha = 2.9°$, $C_L = .9$, gear down.

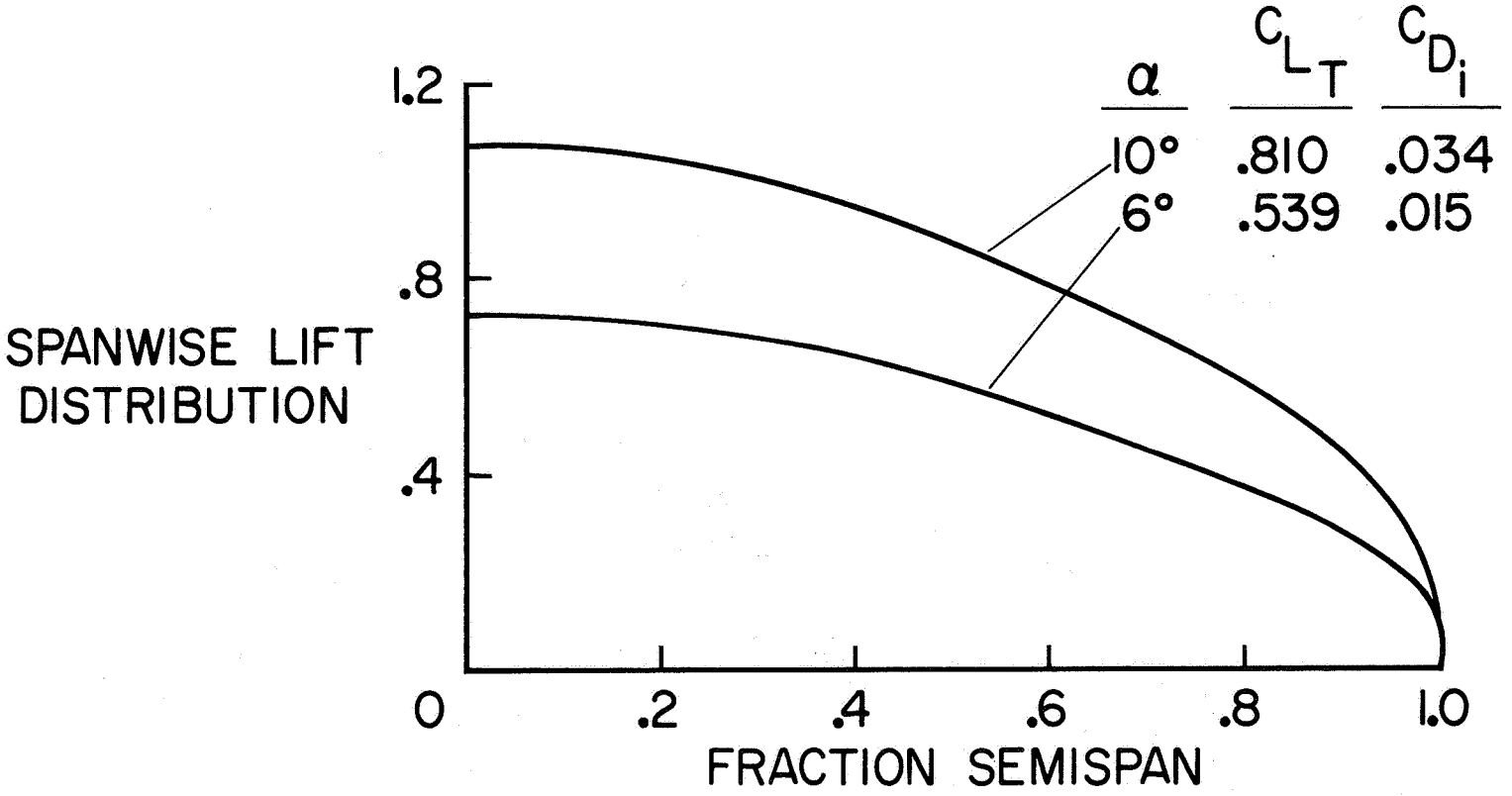

Figure 13.– Predicted spanwise lift distribution, clean configuration.

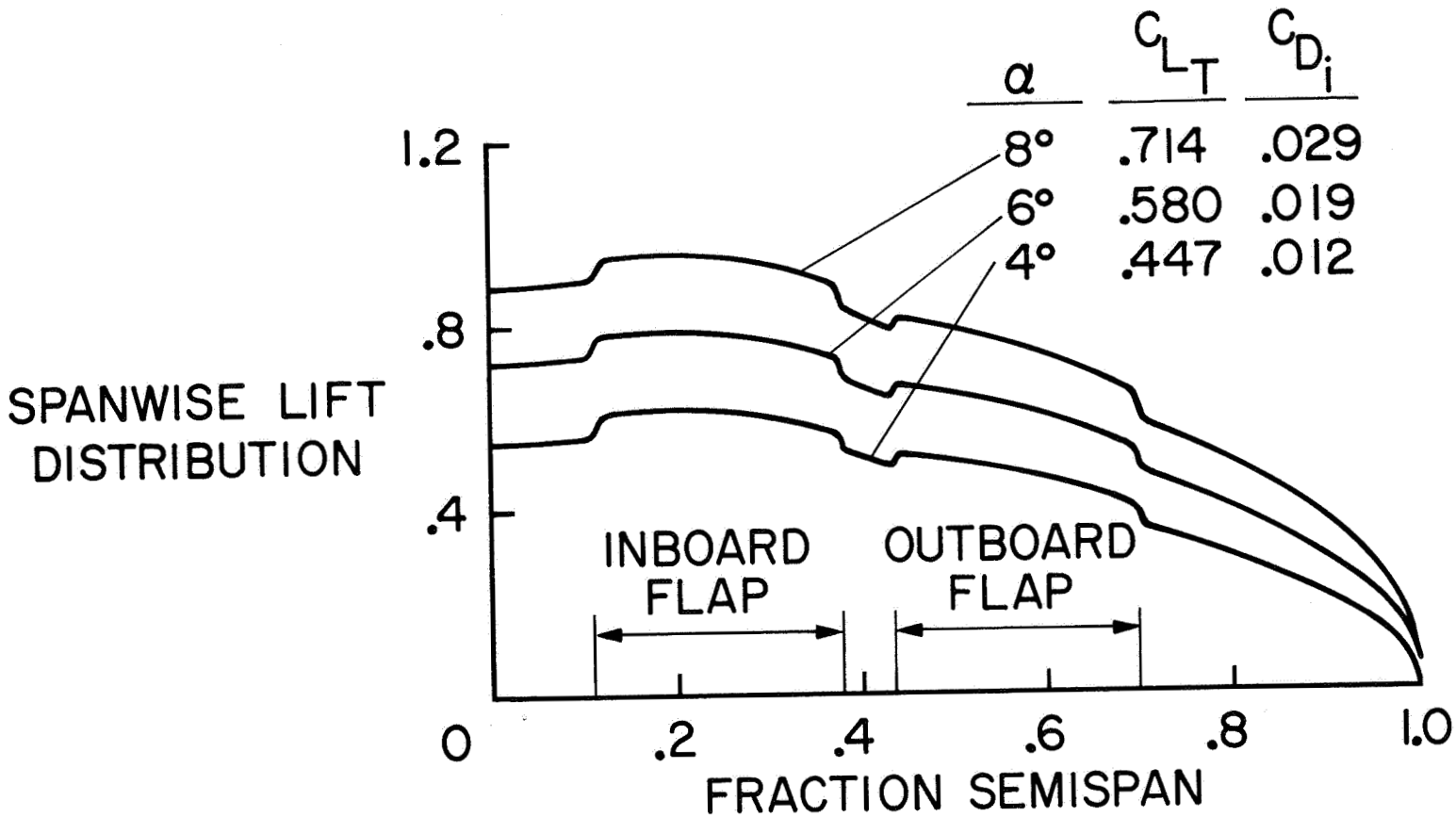

Figure 14.– Predicted spanwise lift distribution, take-off configuration.

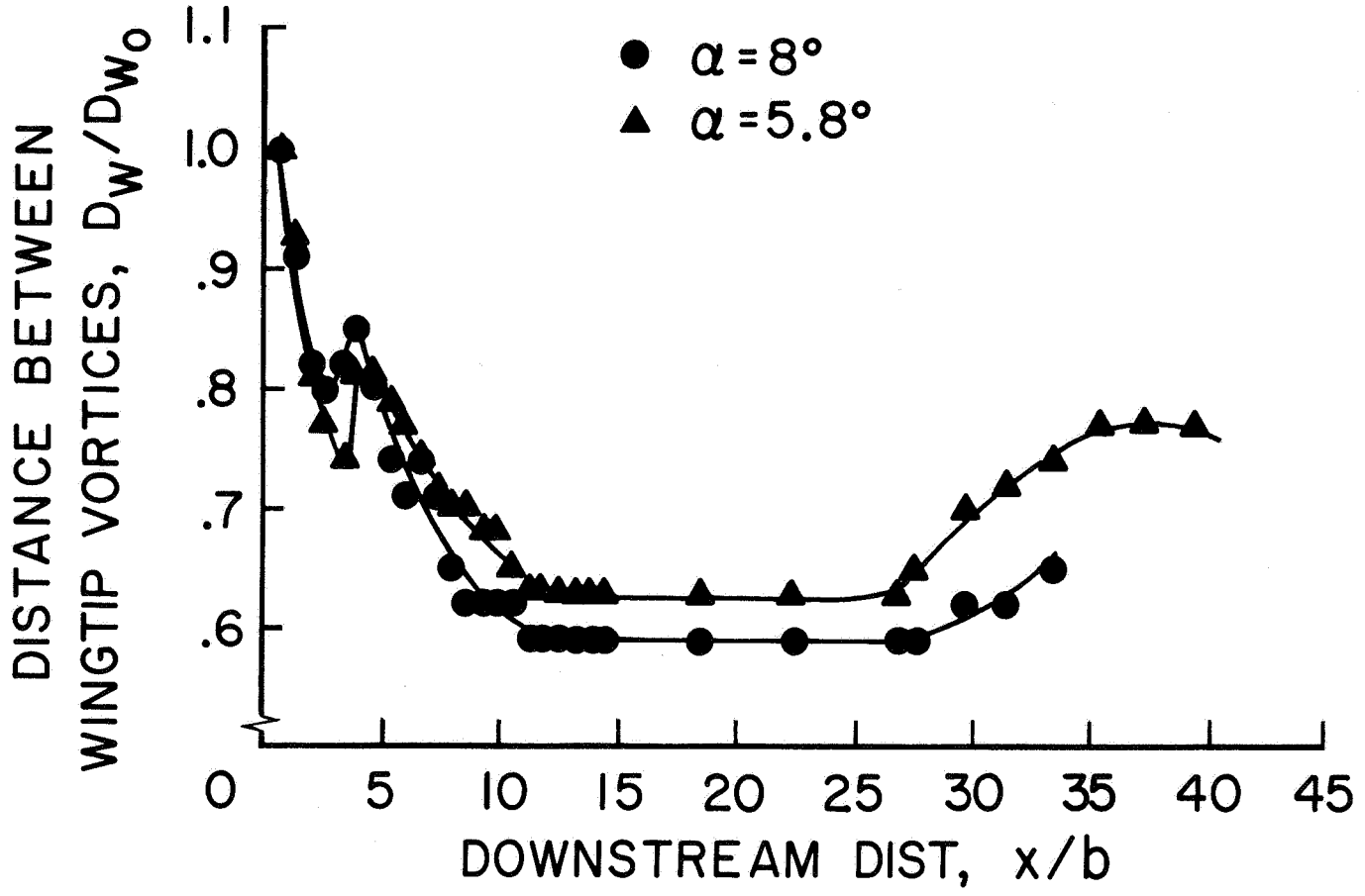

Figure 15.– Spacing between wing tip vortices vs. downstream distance; T.O. configuration, gear down.

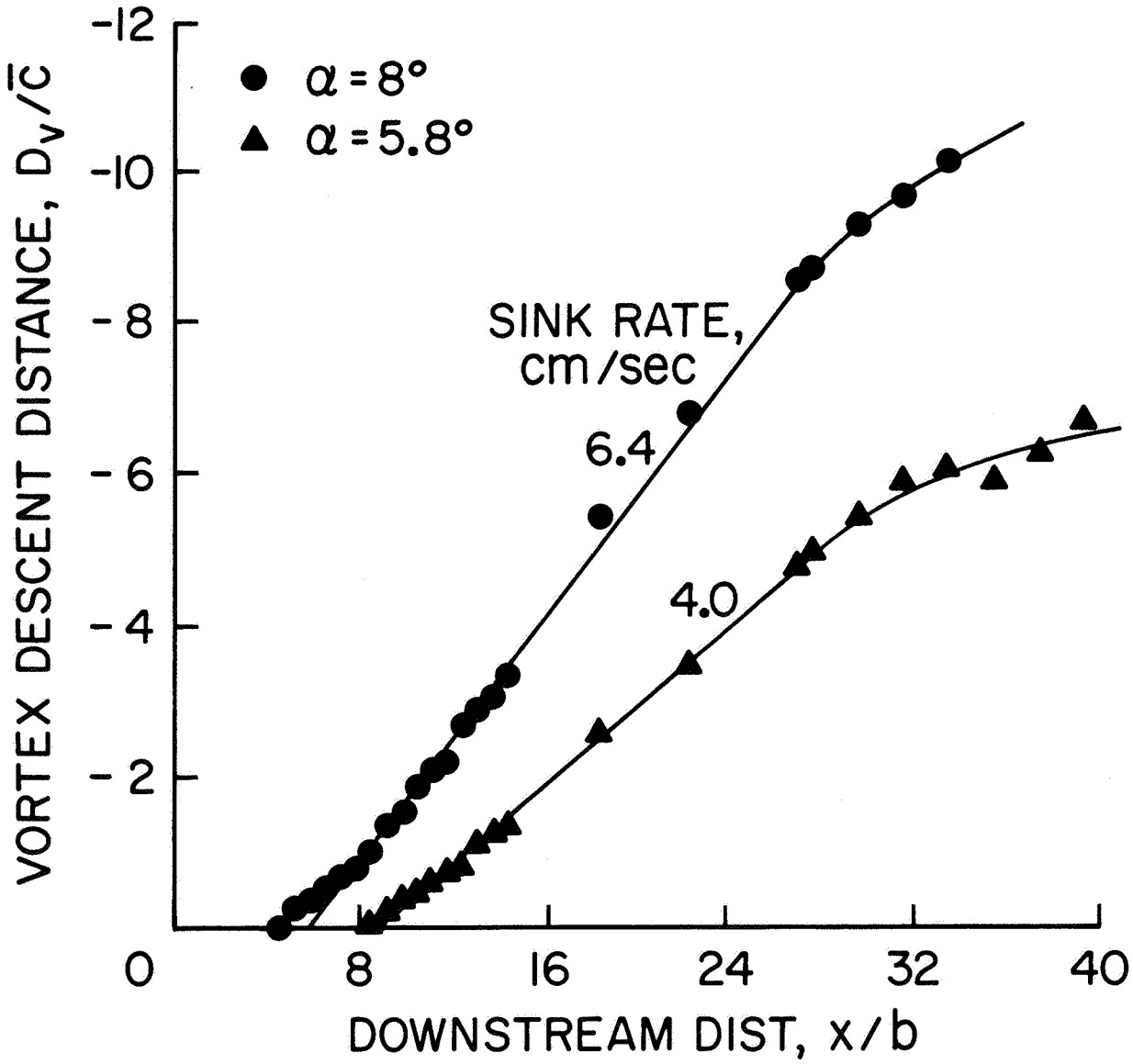

Figure 16.– Vertical descent distance vs. downstream distance; T.O. configuration, gear down.

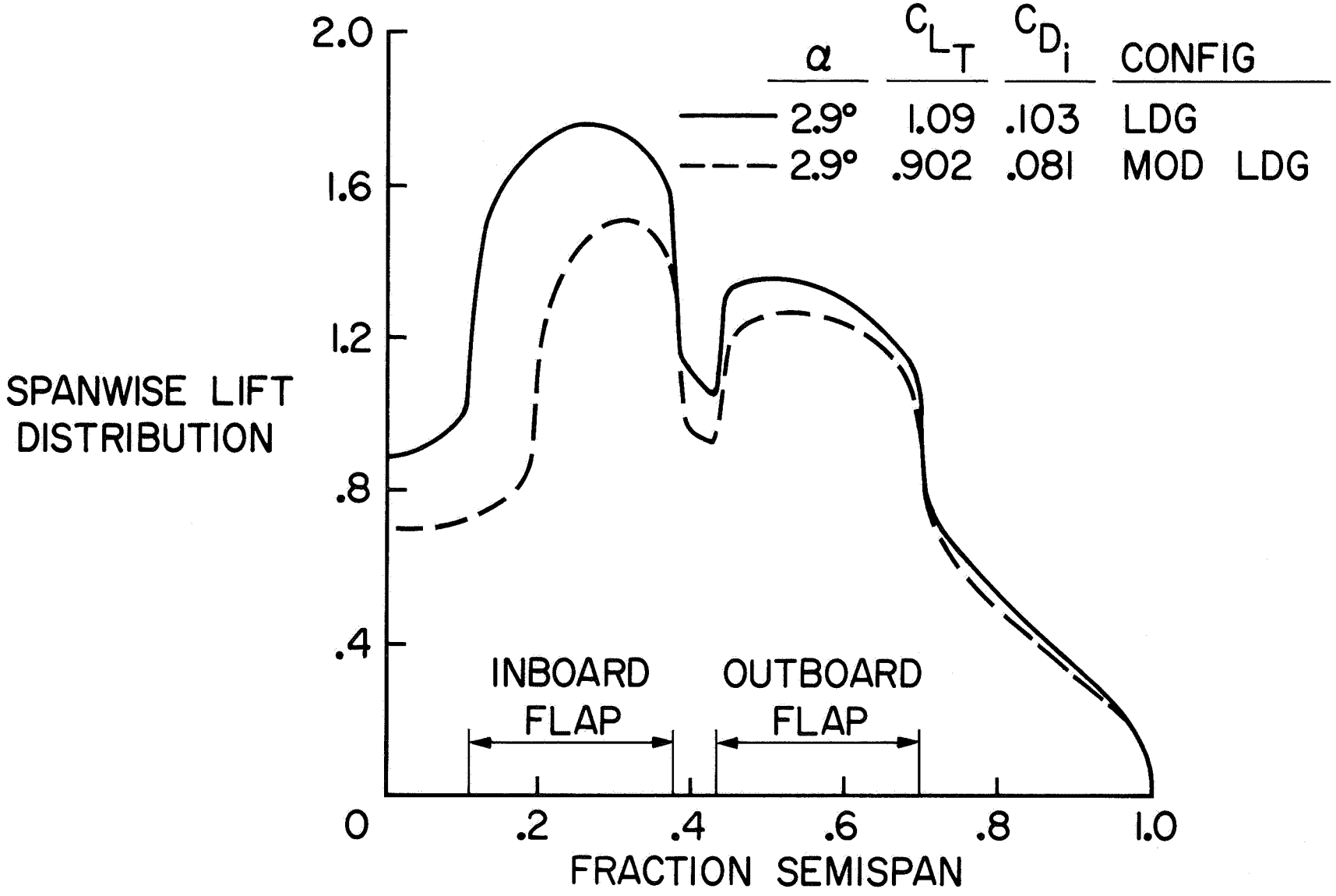

Figure 17.– Predicted spanwise lift distribution, landing and modified landing configurations.

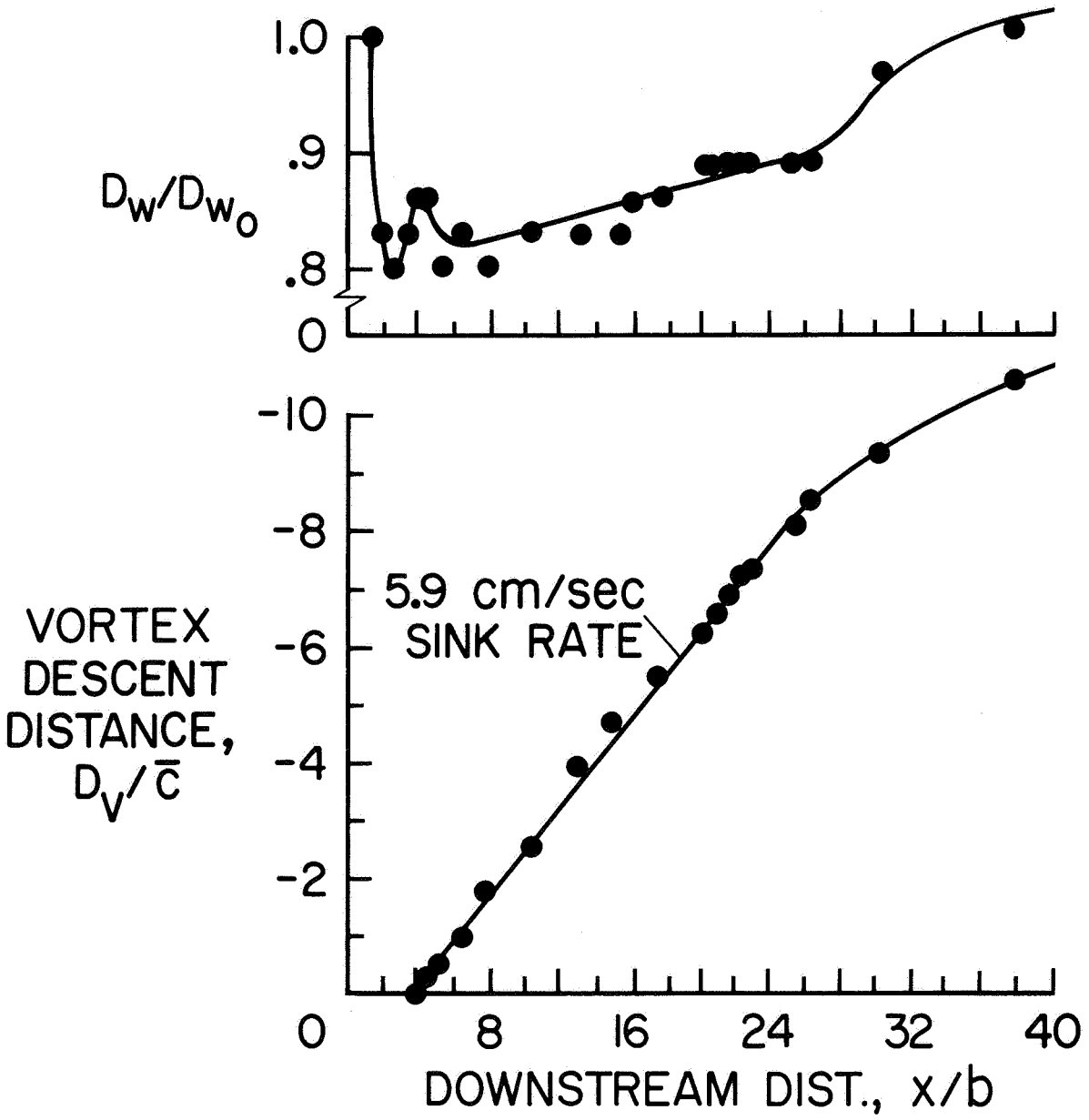

Figure 18.– Vertical descent distance and spacing between wing tip vortices vs. downstream distance; LDG configuration, gear down, $\alpha = 2.9°$.

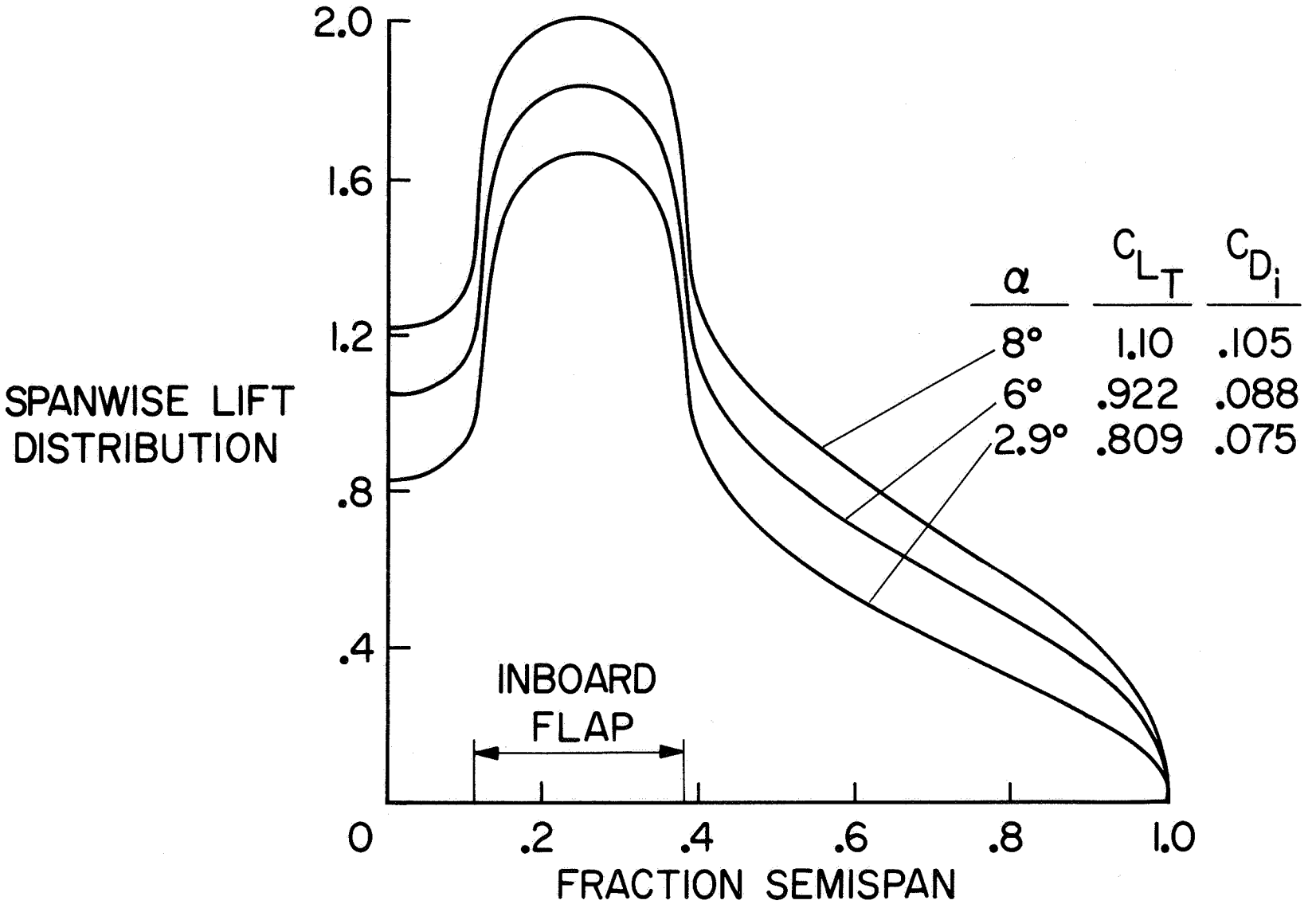

Figure 19.– Predicted spanwise lift distribution; LDG/O configuration.

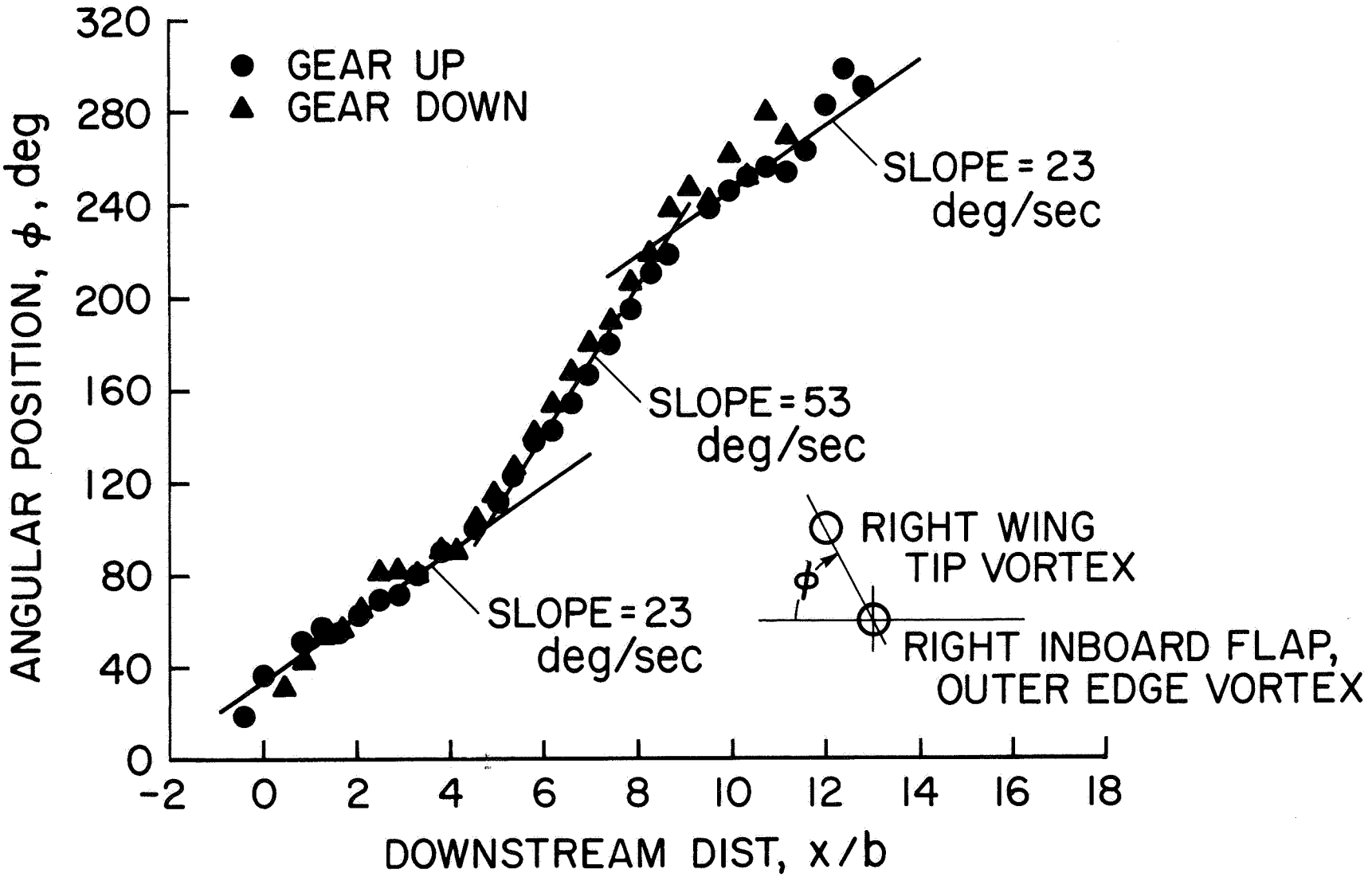

Figure 20.– Angular position of wing tip vortex with respect to flap outer edge vortex vs. downstream distance, LDG/O configuration, $\alpha = 5.8°$.

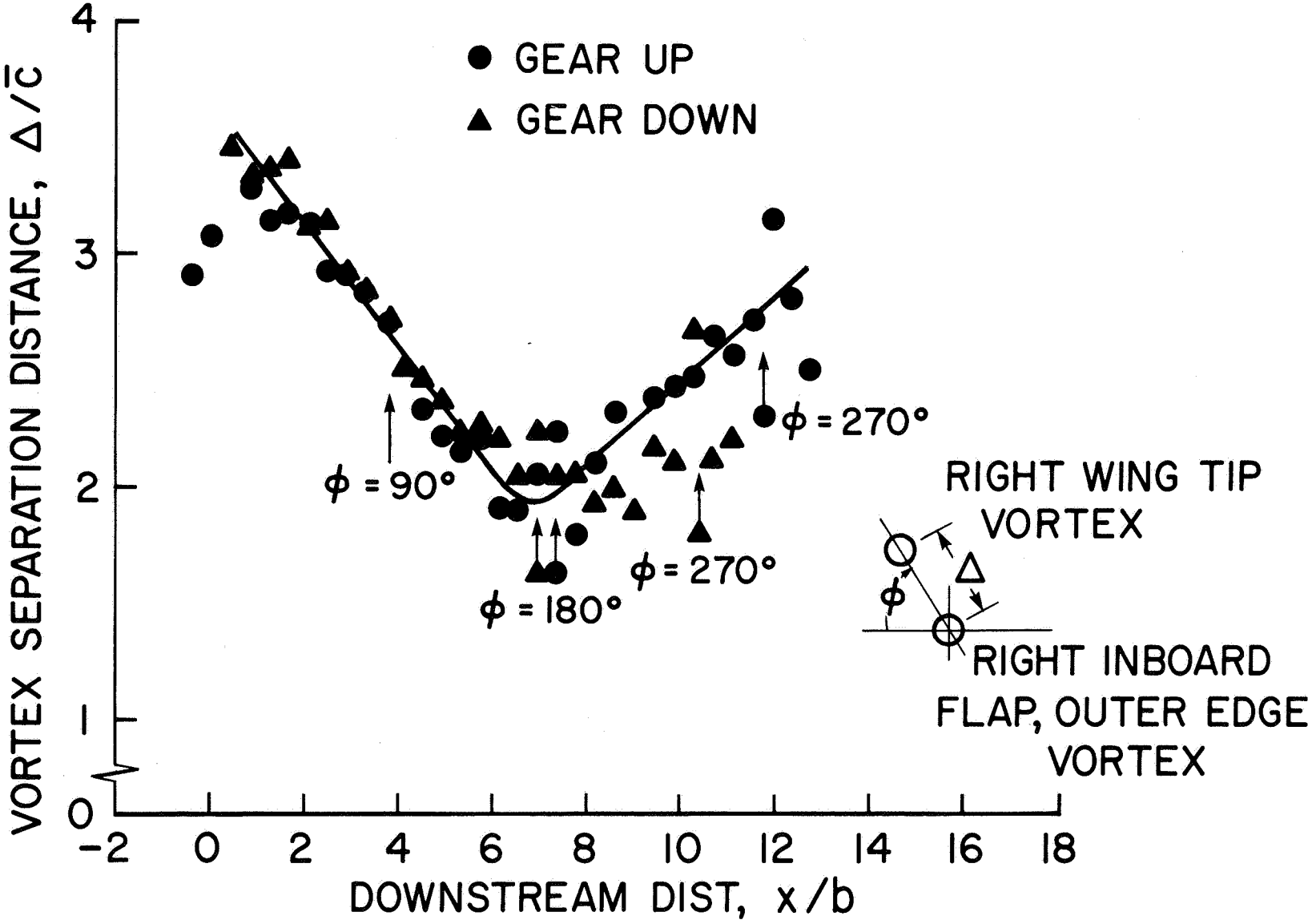

Figure 21.– Measured distance between wing tip vortex and flap outer edge vortex; LDG/O configuration, $\alpha = 5.8°$.

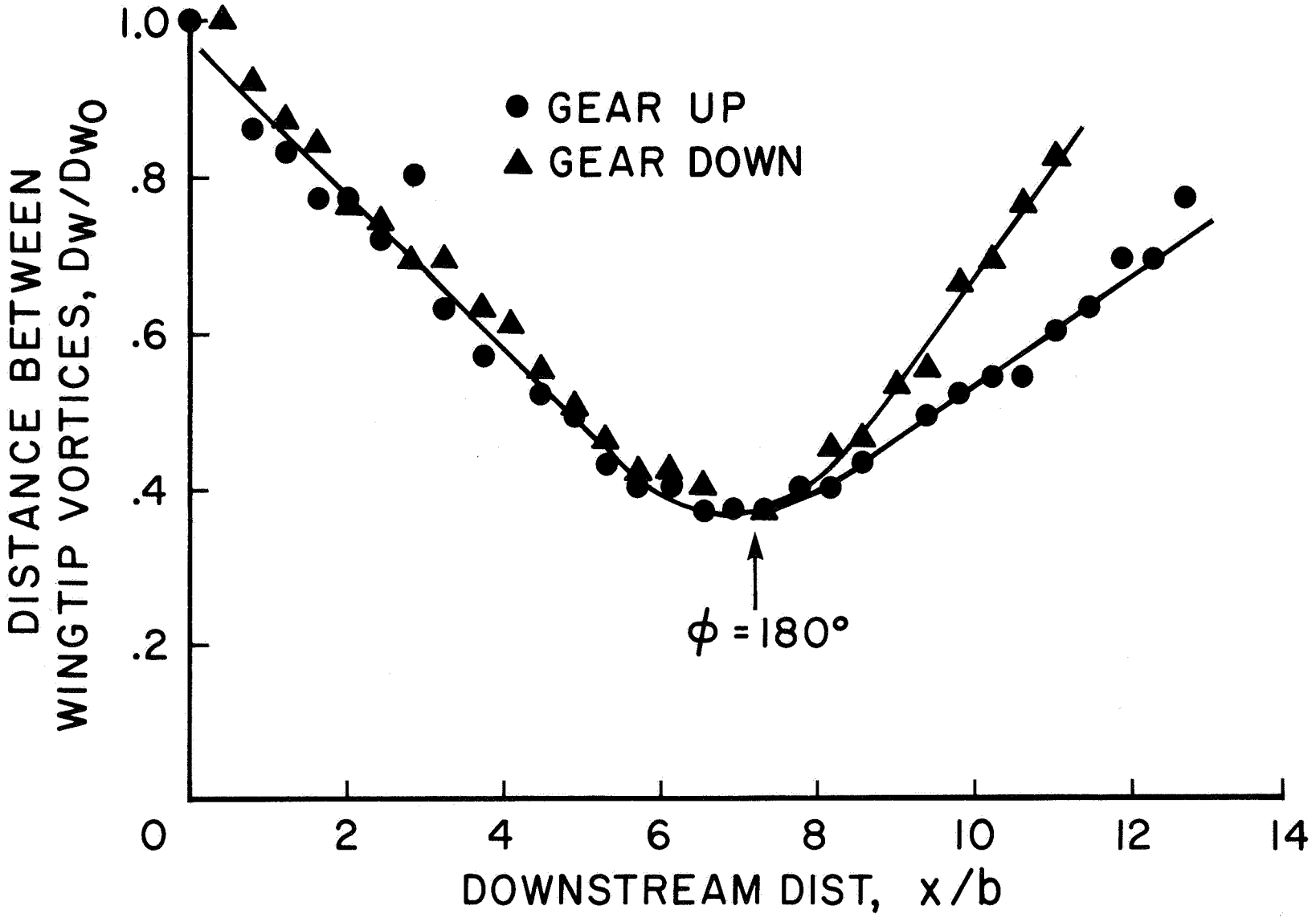

Figure 22.– Spacing between wing tip vortices vs. downstream distance; LDG/O configuration, $\alpha = 5.8°$.

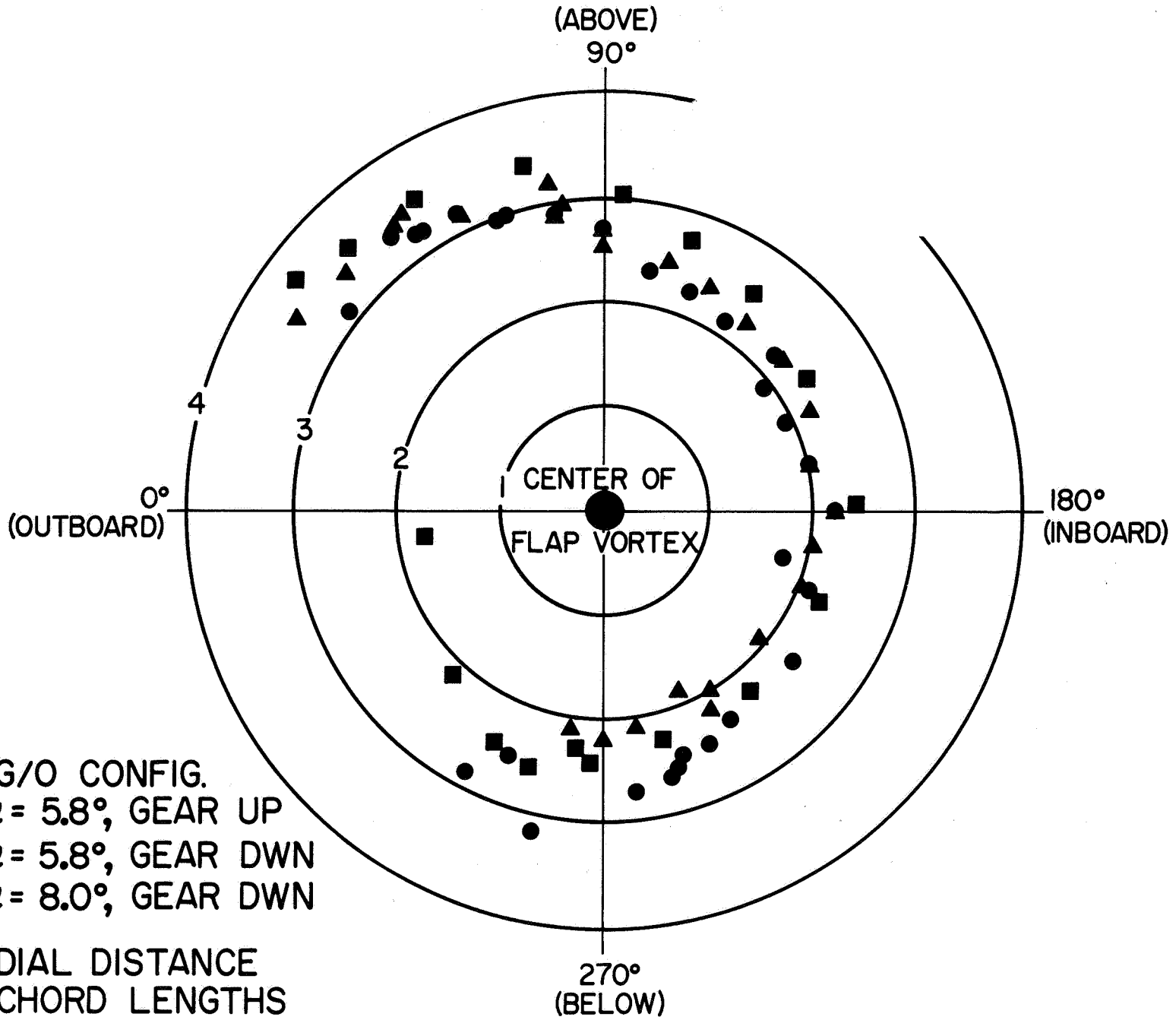

Figure 23.— Trajectory of right wing tip vortex as it orbits and merges with vortex shed from outboard edge of right inboard flap.

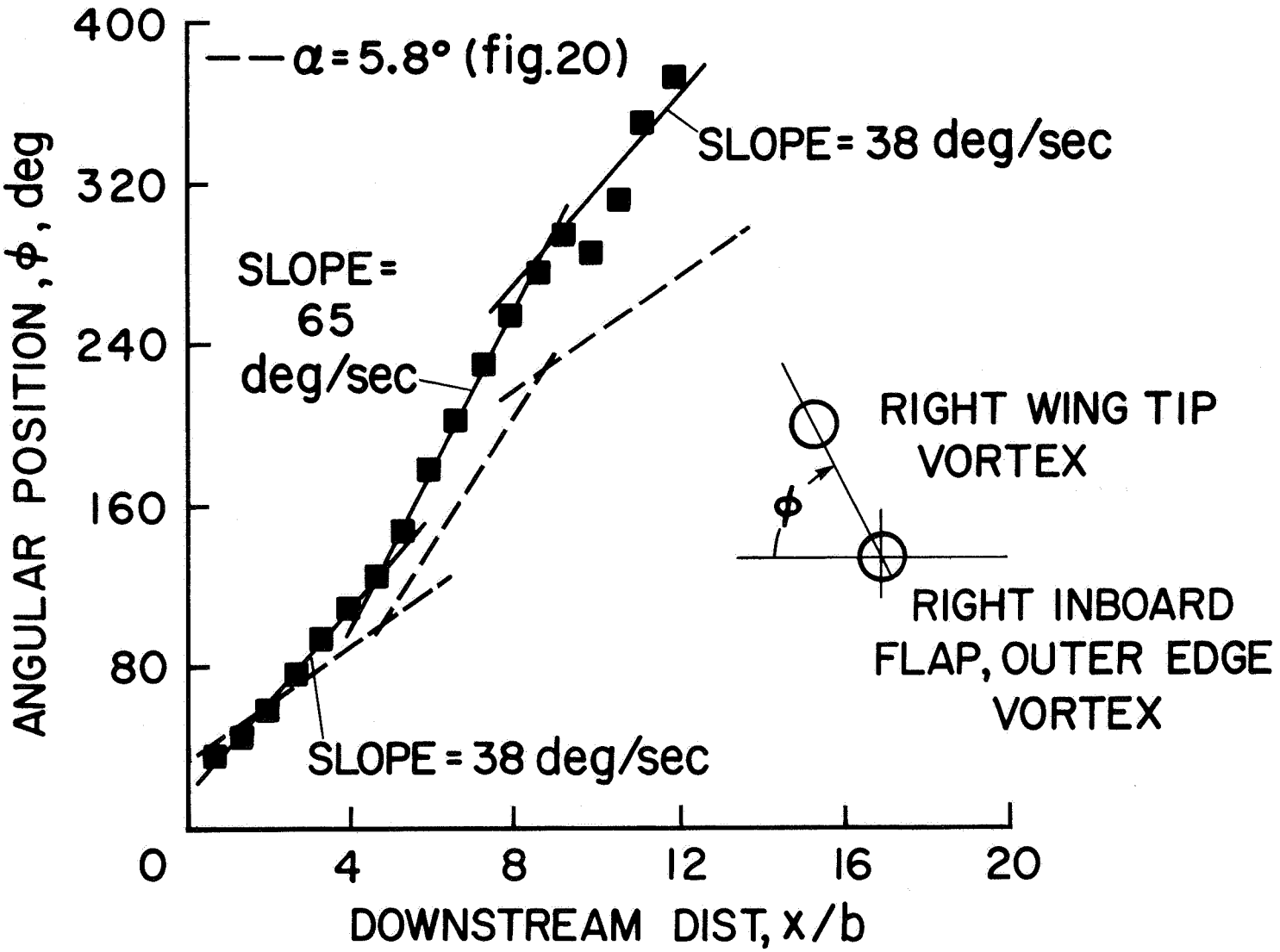

Figure 24.– Angular position of wing tip vortex with respect to flap outer edge vortex vs. downstream distance; LDG/O configuration, $\alpha = 8°$, gear down.

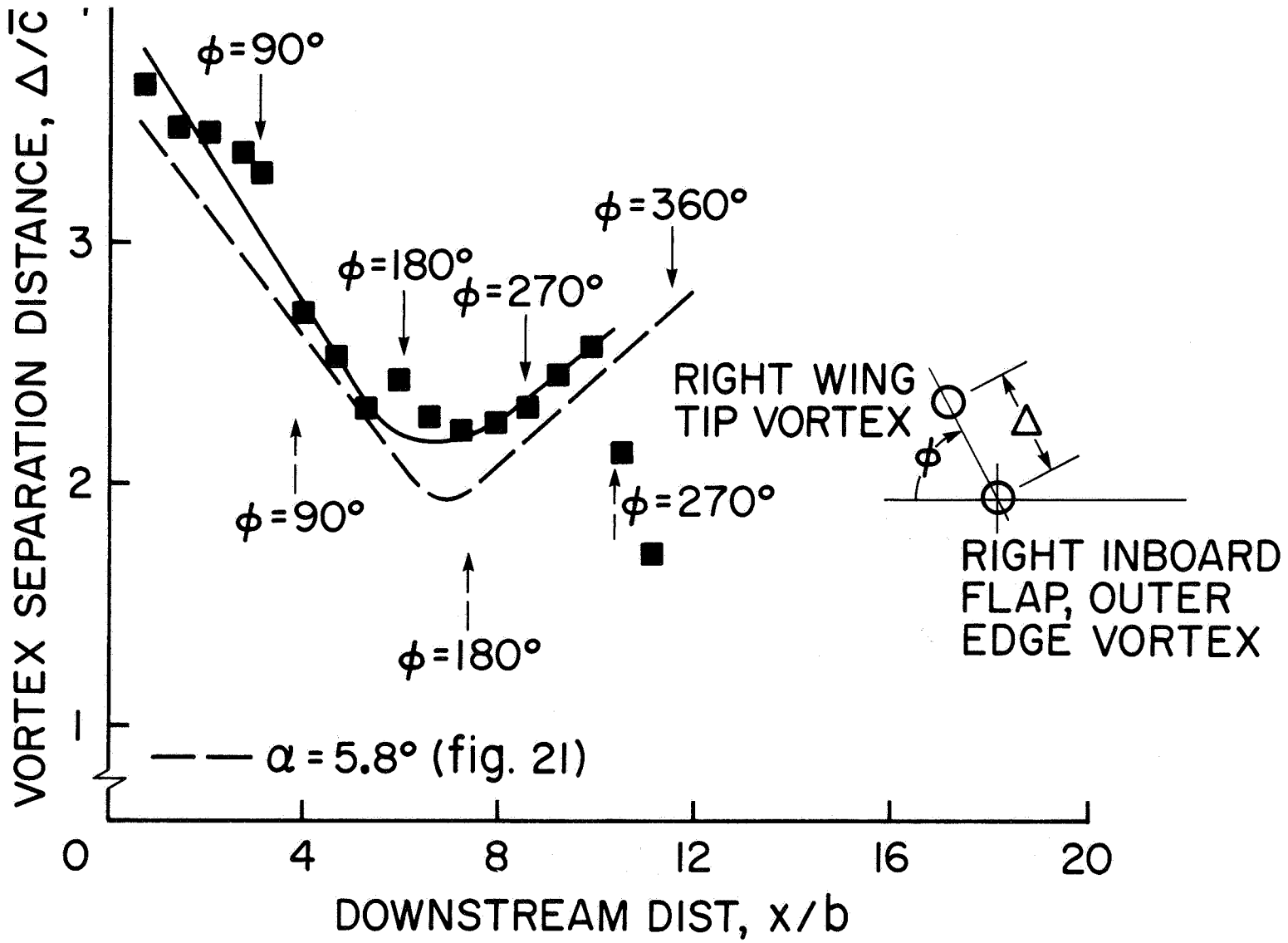

Figure 25.– Measured distance between wing tip vortex and flap outer edge vortex vs. downstream distance; LDG/O configuration, $\alpha = 8°$, gear down.

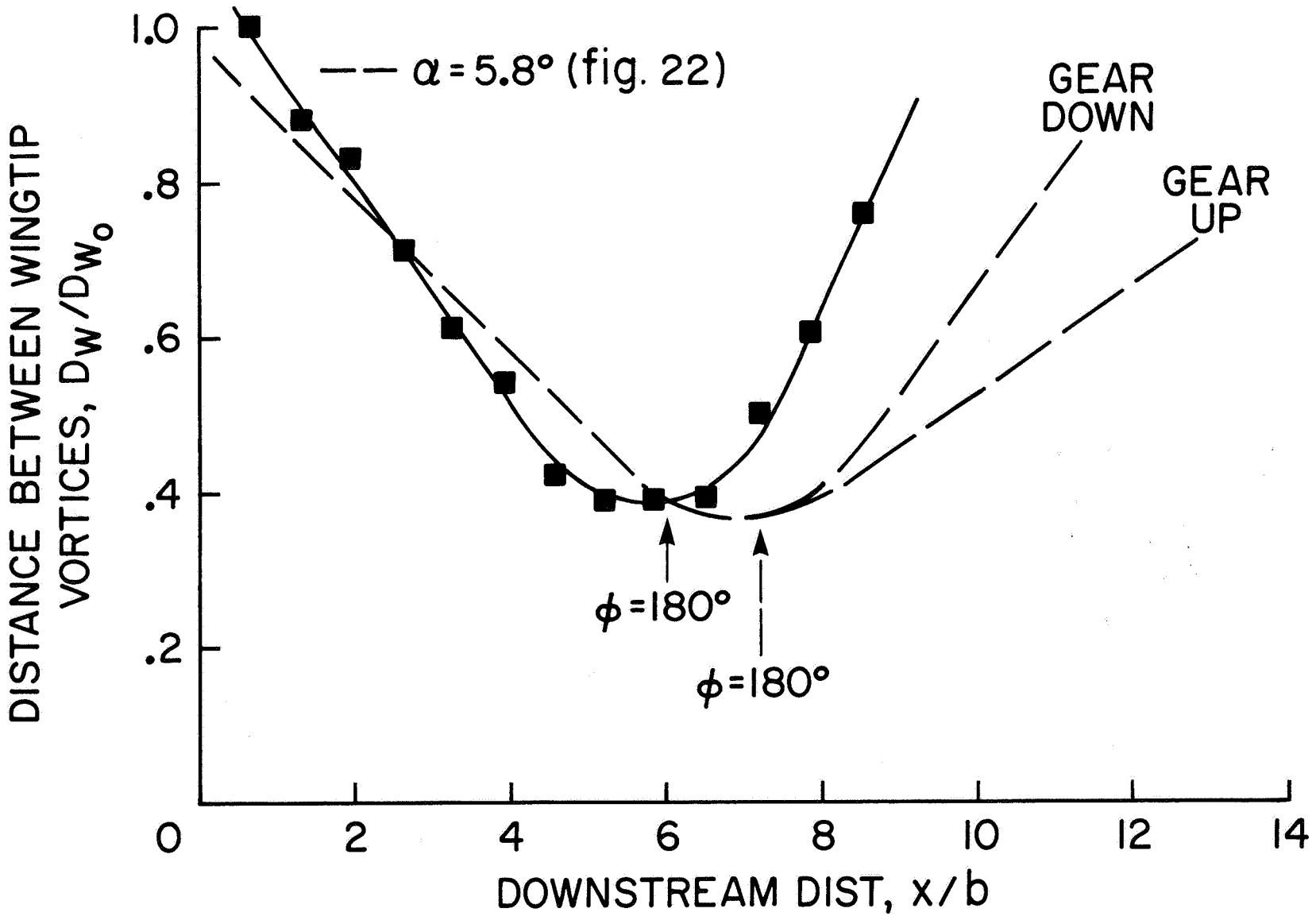

Figure 26.– Spacing between wing tip vortices vs. downstream distance, LDG/O configuration, $\alpha = 8°$, gear down.

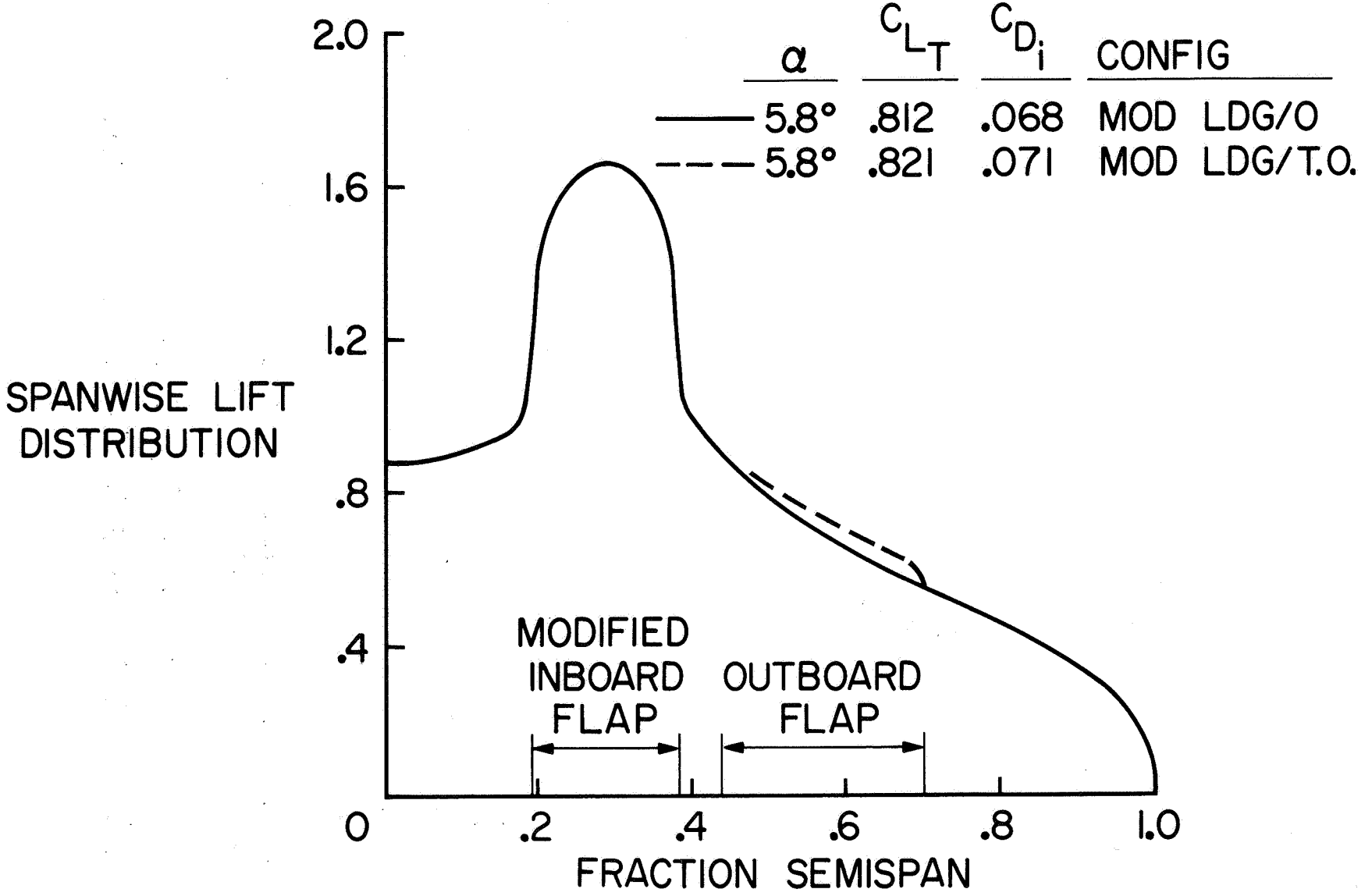

Figure 27.— Predicted spanwise lift distribution, modified LDG/O and modified LDG/T.O. configurations.

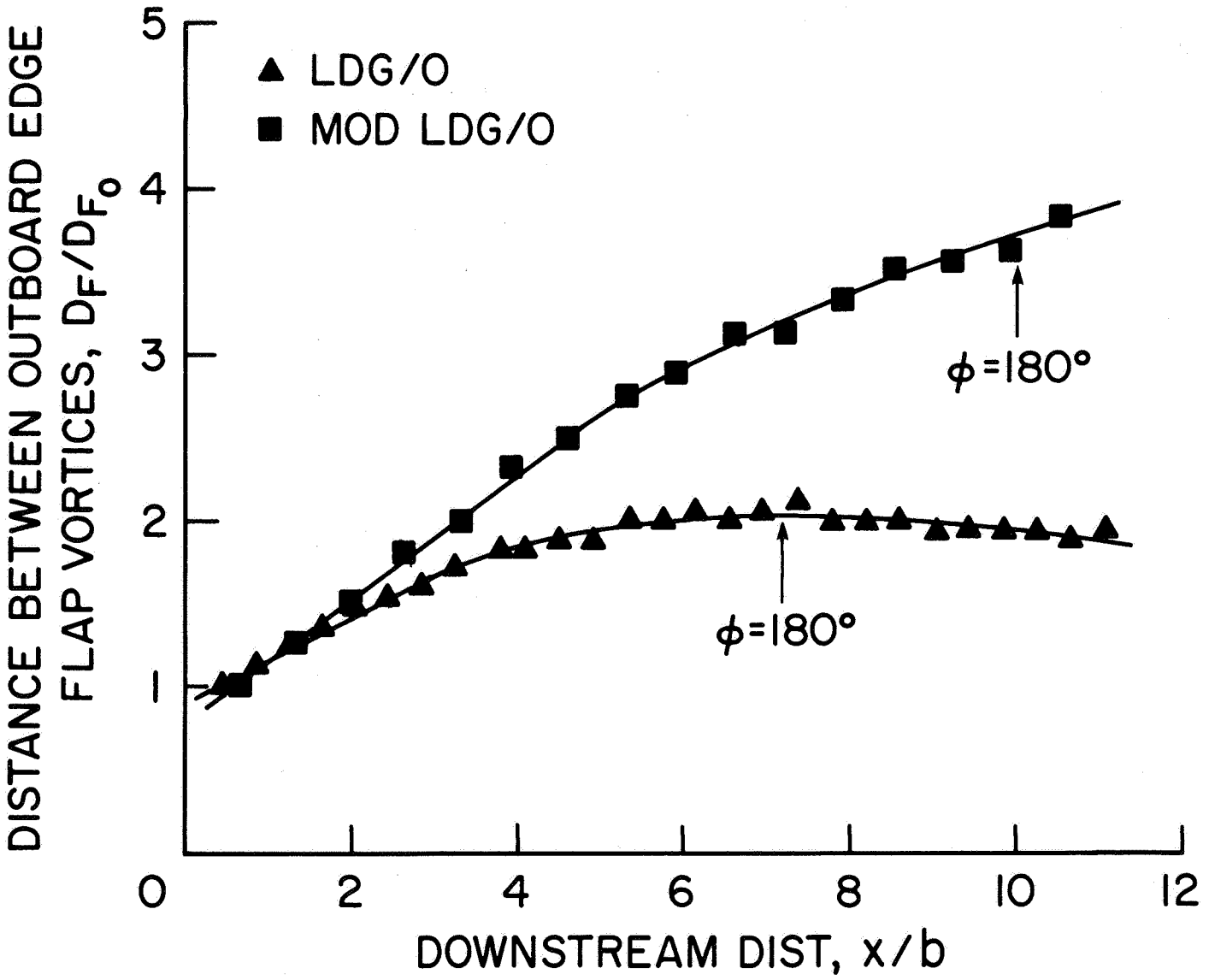

Figure 28.– Distance between outboard edge flap vortices, MOD LDG/O and LDG/O configurations, $\alpha = 5.8°$, gear down.

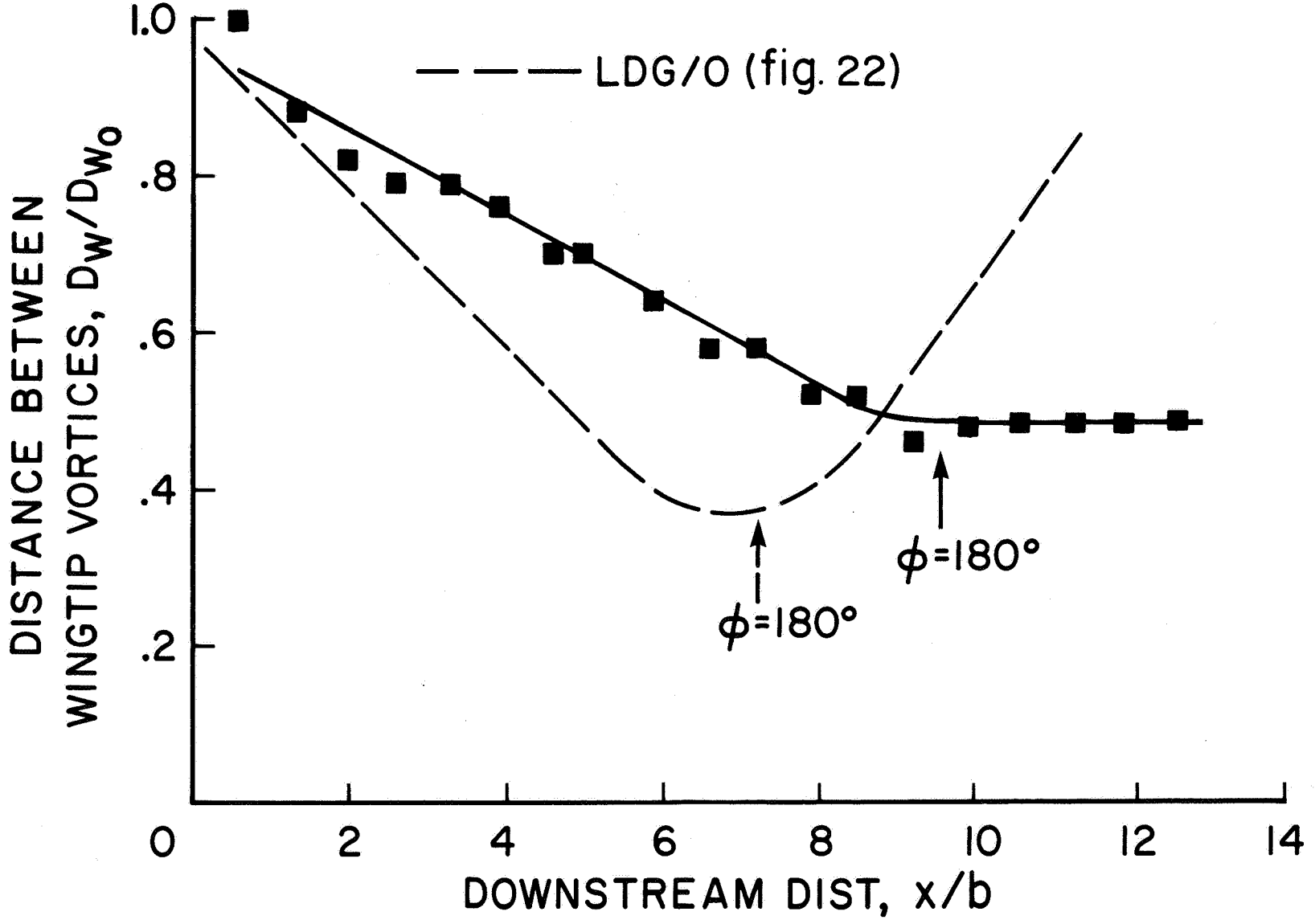

Figure 29.– Spacing between wing tip vortices vs. downstream distance, MOD LDG/O configuration, $\alpha = 5.8°$, gear down.

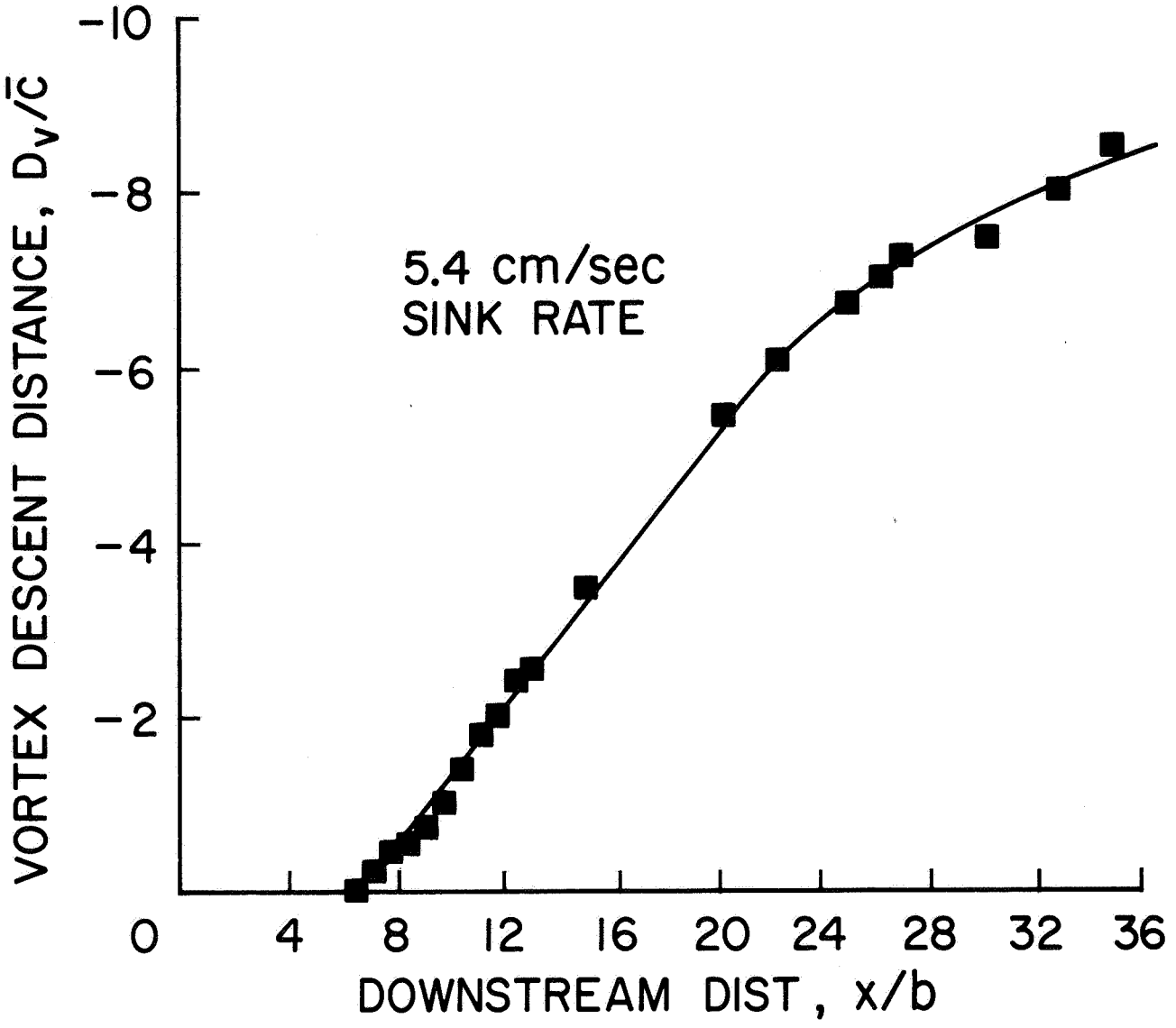

Figure 30.– Vertical descent distance vs. downstream distance, MOD LDG/O configuration, $\alpha = 5.8°$, gear down.

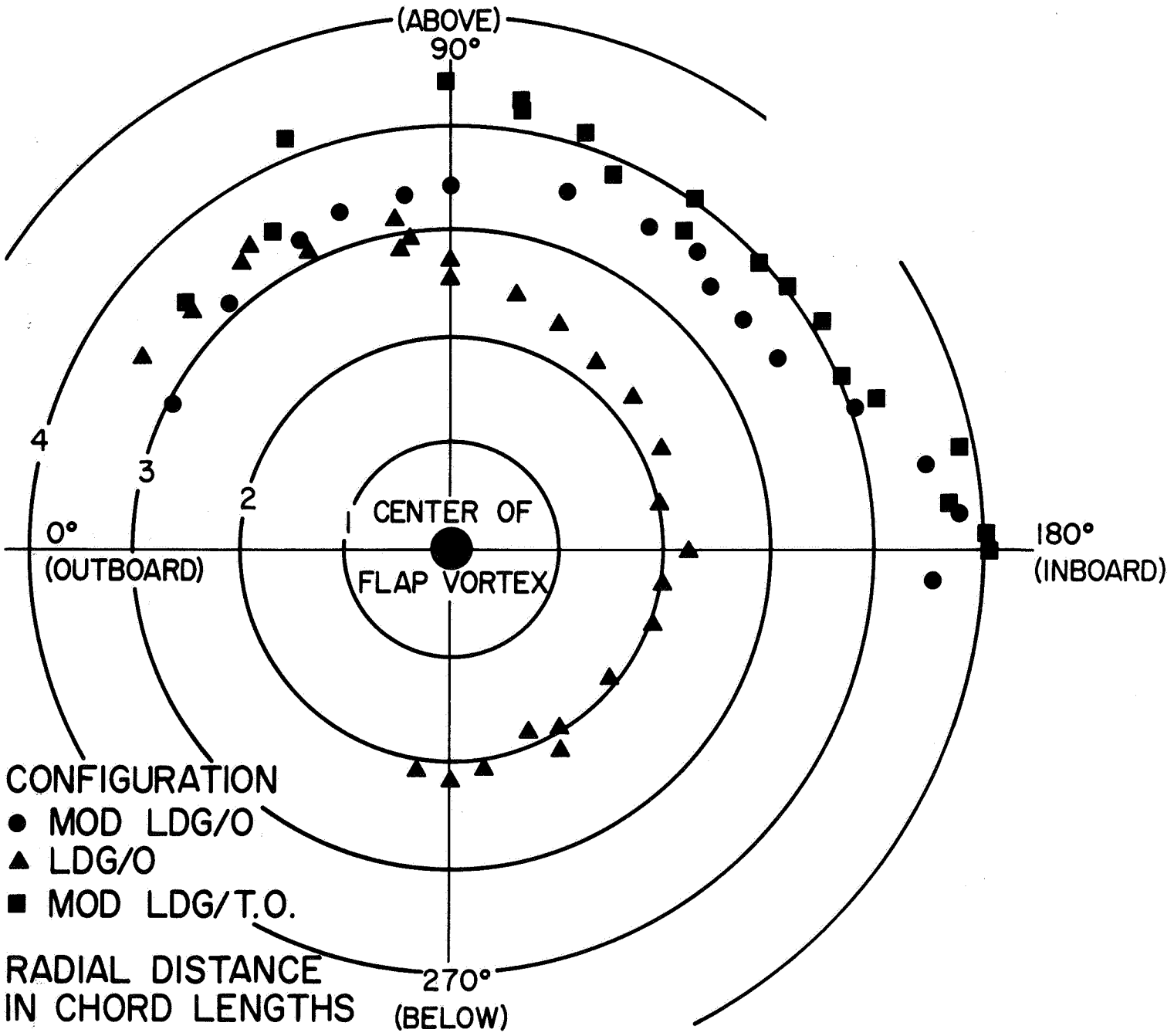

Figure 31.– Trajectory of right wing tip vortex as it orbits and merges with vortex shed from outboard edge of right inboard flap, $\alpha = 5.8°$, gear down.

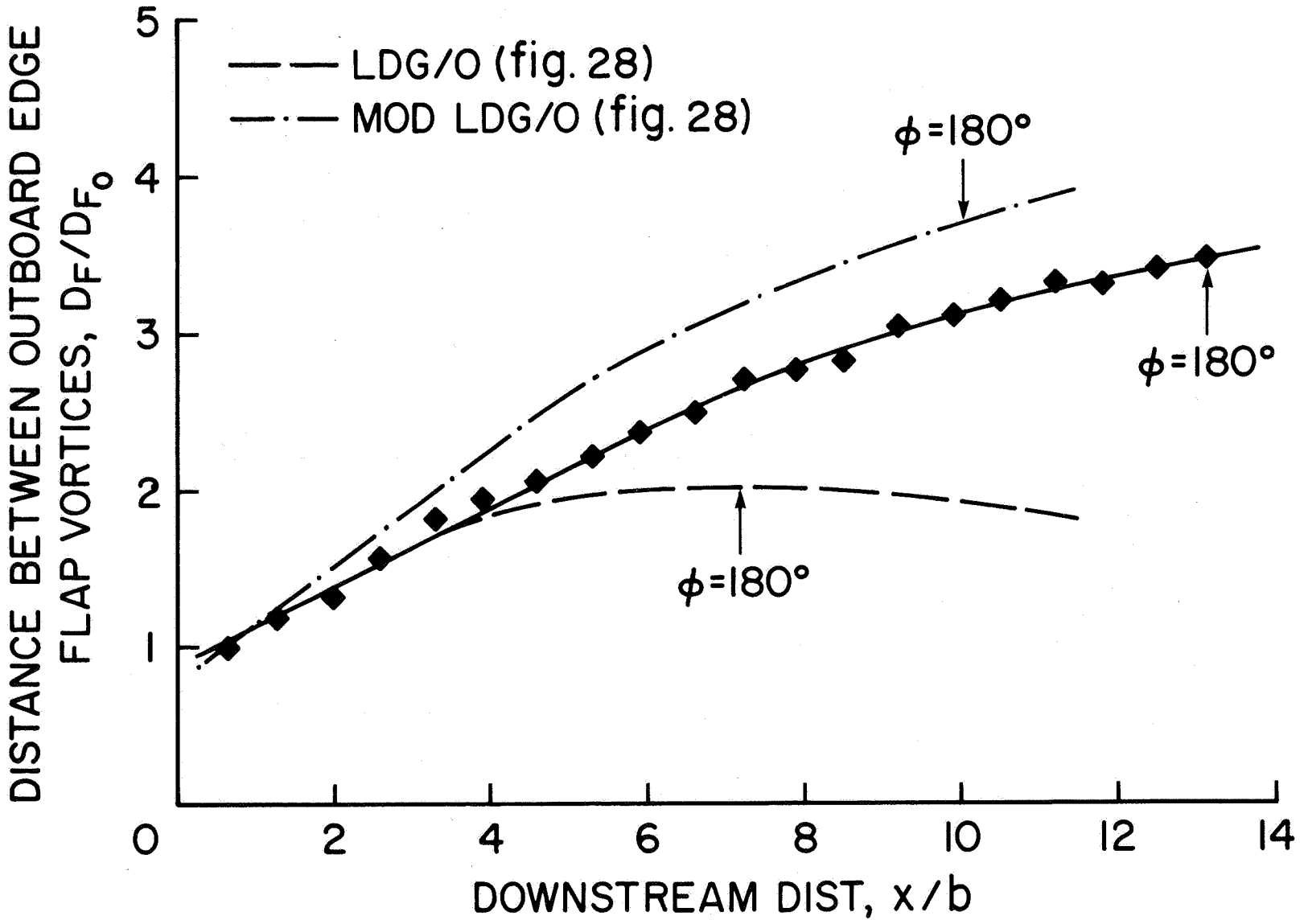

Figure 32.– Distance between outboard edge flap vortices, MOD LDG/T.O. configuration, $\alpha = 5.8°$, gear down.

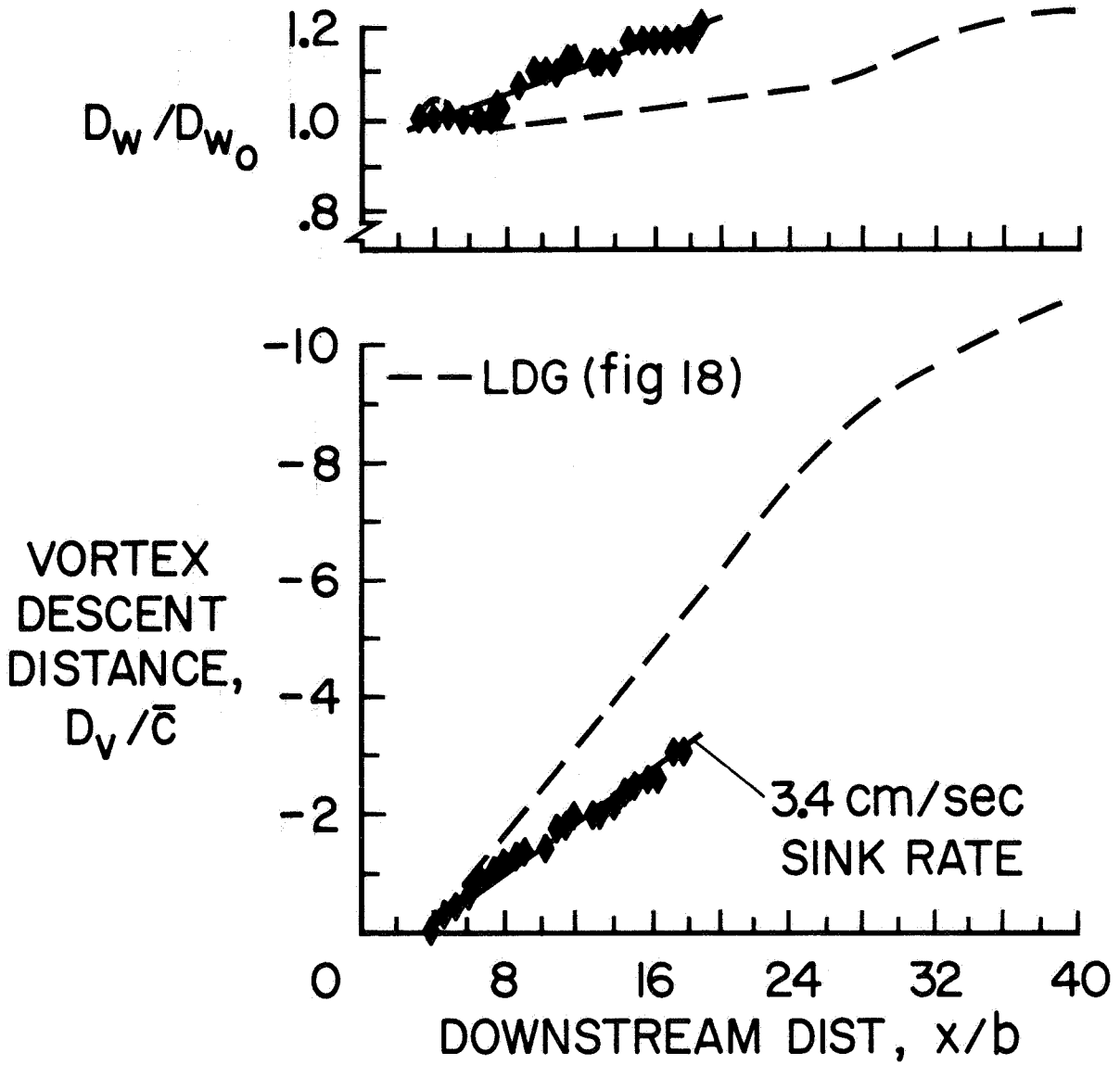

Figure 33.– Vertical descent distance and spacing between wing tip vortices vs. downstream distance, MOD LDG configuration, $\alpha = 2.9°$, gear down.